Article

Not peer-reviewed version

Salinity Fronts in the South Atlantic

Igor M Belkin * and Xin-Tang Shen

Posted Date: 18 March 2024

doi: 10.20944/preprints202403.0975.v1

Keywords: sea surface salinity; remote sensing; ocean fronts; SMOS; South Atlantic

Article

Salinity Fronts in the South Atlantic

Igor M. Belkin * and Xin-Tang Shen

College of Marine Science and Technology, Zhejiang Ocean University, Zhoushan 316022, China
* Correspondence: igormbelkin@gmail.com

Abstract: Seasonal climatology of salinity fronts in the South Atlantic has been created from satellite SMOS sea surface salinity (SSS) measurements, 2011-2019, processed at the Barcelona Expert Center of Remote Sensing (BEC) and provided as high-resolution (1/20°) SSS data. The SSS fronts are identified with narrow zones of enhanced horizontal gradient magnitude (GM) of SSS computed with the Belkin-O'Reilly algorithm. Seasonal climatologies are generated for large-scale open-ocean SSS fronts and for low-salinity regions maintained by the Rio de la Plata discharge, Magellan Strait outflow, Congo River discharge, and Benguela upwelling. To facilitate feature recognition in satellite imagery, the salinity gradient has been log-transformed, which improved visual contrast of gradient maps, revealing new features. A 2000-km-long triangular area in the eastern tropical-subtropical Atlantic is filled with regular quasi-meridional mesoscale striations that form a giant ripple field with a 100-km wave length extending from Africa toward the NE Brazil. South of the Tropical Front, within the subtropical high-salinity pool, a trans-ocean quasi-zonal narrow linear belt of SSS maximum is documented. The Smax belt shifts north-south seasonally while retaining its well-defined linear morphology, which is suggestive of a mechanism that maintains this feature. In the SW Atlantic, the Rio de la Plata plume expands in winter (June-July), reaching across the South Brazilian Bight, up to Cabo Frio (23°S) and beyond. The Plata estuarine front moves in and out seasonally. Farther south, the Magellan Strait outflow expands northward in winter up to 39-40°S to nearly join the Plata outflow. In the SE Atlantic, the Congo River plume spreads radially from the river mouth, with the spreading direction varying seasonally and interannually. The plume is often bordered from the south by a quasi-zonal front along 6°S. The diluted Congo River water spreads southward seasonally down to the thermal Angola-Benguela Front at 16°S. The Benguela upwelling is delineated by a meridional front, which extends north alongshore up to 20°S, where the low-salinity Benguela upwelling water meets the high-salinity tropical water ("Angola water") to form a salinity front, which is separate from the thermal Angola-Benguela Front at 16°S. The Angola water thus forms a wedge between the low-salinity waters of the Congo River outflow in the north and Benguela upwelling in the south. This high-salinity wedge is bordered by salinity fronts that migrate north-south seasonally.

Keywords: sea surface salinity; remote sensing; ocean fronts; SMOS; South Atlantic

1. Introduction

Foreword: Remote sensing of salinity fronts on a global scale began in this century owing to three satellite missions – SMOS, Aquarius, and SMAP – that carried radiometers whose data are used to estimate sea surface salinity (SSS; Reul et al., 2014; Boutin et al., 2018; Vinogradova et al., 2019; Reul et al., 2020; Boutin et al., 2021; Boutin et al., 2023). The SSS data from all three missions have been used, albeit sporadically, to study space-time variability of *salinity fronts*, mostly in the tropics (Qu et al., 2014; Kao and Lagerloef, 2015; Yu, 2015; Melnichenko et al., 2016; Nyadjro and Subrahmanyam, 2016; Asto et al., 2019; Reul et al., 2020; Bao et al., 2021; Boutin et al., 2023, pp. 1469-1471; Vazquez-Cuervo et al., 2023). Yet, despite the proven potential of satellite SSS data, the global climatology of salinity fronts is lacking. The potential importance of such climatology was the main impetus for this study. We choose to focus first on fronts of the Southern Hemisphere because they are less studied compared with fronts of the Northern Hemisphere. The present report on the South Atlantic will be followed by similar reports on the South Indian and South Pacific oceans. The structure of this paper is as follows: Section 1 introduces numerous South Atlantic fronts and remote sensing studies of these fronts, thereby providing a background for our study. Satellite SSS data and data processing are

 doi:10.20944/preprints202403.0975.v1

described in Section 2. Results are presented in Section 3, followed by the Discussion in Section 4 and Conclusions in Section 5.

Remote sensing of ocean fronts in the South Atlantic: The seminal survey of sea surface temperature (SST) fronts by Legeckis (1978) ushered in an era of remote sensing studies of ocean fronts. Table 1 provides a provisional inventory of remote sensing studies of the South Atlantic, followed by a brief regional introduction to the most important studies of fronts and frontal zones of this vast region, between the equator and Antarctic Circumpolar Current (ACC).

Table 1. Satellite studies of the South Atlantic.

Reference	Variable	Period	Sensor/Mission	Region
Allega et al. 2021	SST	1985-2019	AVHRR, MODIS	Patagonian Shelf
Artana et al. 2018	SST, SSH	2007-2016	Multisensor; Altimeters	SW Atlantic
Barre et al. 2006	SST, color	2002-2004	MODIS, SeaWiFS	Brazil-Malvinas Confluence
Belkin & Shen 2024 (this study)	SSS	2011-2019	SMOS	South Atlantic (0-60°S)
Billany et al. 2010	SSH	1993-2007	Altimeters	Greenwich Meridian
Bouali et al. 2017	SST	2003-2014	MODIS	South Atlantic (0-60°S)
Burls & Reason 2006	SST	2002-2005	TRMM, AMSR-E	South Atlantic (25 -55°S)
Castellanos et al. 2019	SSS	2011-2015	SMOS	SW Atlantic; SE Atlantic; 12mos
Chao et al. 2015	SSS	2011-2013	Aquarius	Congo River plume
Chen et al. 2019	SST	2002-2016	MODIS	SE Brazil; Shelf fronts
Da Silveira et al. 2023	SST SSH	2002-2020 1993-2020	Multi-sensor Altimeters	Brazil Current, 22-23°S
Dencausse et al. 2011	SSH	1992-2007	Altimeters	SE Atlantic (5°W-35°E)
Dong et al. 2006	SST	2002-2005	AMSR-E	Polar Front
Franco et al. 2008	SST	1985-2002	AVHRR	Patagonian Shelf; SBF (39-44°S)
Franco et al. 2022	SST SSH CHL	1993-2019 1993-2019 2002-2020	Multi-sensor Altimeters MODIS	Patagonian Shelf
Freeman & Lovenduski 2016	SST	2002-2014	Microwave radiometers	Polar Front
Graham & de Boer 2013	SST SSH	1999-2009 1999-2009	AVHRR Altimeters	Subtropical Front
Guerrero et al. 2014	SSS	2010-2013 2011-2013	SMOS Aquarius	SW Atlantic
Hopkins et al. 2013	SST SSS CHL SSH	2010	AVHRR, AMSR SMOS MODIS, MERIS Altimeters	Congo River plume
Hösen et al. 2016	SST	2006-2011 2011-2014	AMSR-E/MODIS 9 km MODIS 4 km	Benguela upwelling filaments
Houndegnonto et al. 2021	SSS	2010-2017	SMOS	Congo River plume
Kim & Orsi 2014	SSH	1992-2011	Altimeters	ACC fronts
Legeckis & Gordon 1982	SST	1975-1978	VHRR	Brazil-Malvinas Confluence
Lorenzzetti et al. 2009	SST	2000-2002	AVHRR	Brazil Current
Luko et al. 2021	Velocity	1993-2018	Altimeters	South Equatorial Current

 doi:10.20944/preprints202403.0975.v1

Lutjeharms & Meeuwis 1987	SST	1982-1985	AVHRR	SE Atlantic; Benguela upwelling
Lutjeharms et al. 1993	SST	1988	AVHRR	Subtropical Front
Martins & Stammer 2022	SSS	2010-2020	SMOS, Aquarius, SMAP	Congo River plume
Meeuwis & Lutjeharms 1990	SST	1982-1985	AVHRR	Angola-Benguela Current
Melnichenko et al. 2016	SSS	2011-2015	Aquarius	Global
Meeuwis 1991	SST	1982-1985	AVHRR	South Atlantic and South Indian
Moore et al. 1997	SST	1987-1988	AVHRR	Polar Front, 90°W-20°W
Moore et al. 1999	SST	1987-1993	AVHRR	Polar Front, Circumpolar
Olson et al. 1988	SST	1981-1987	AVHRR	Brazil-Malvinas Confluence
Piola et al. 2008a	CHL	1998-2005	SeaWiFS	Rio de la Plata plume
Reul et al. 2014	SSS	2010-2012	SMOS	Congo River plume Fig10
Rivas 2010	SST	1985-2002	AVHRR	Southwest Atlantic
Rivas & Pisoni 2010	SST	1985-2002	AVHRR	Patagonian Shelf
Ruiz-Etcheverry & Saraceno 2020	SSH	1993-2017	Altimeters	South Atlantic (36-55°S)
Saraceno et al. 2004	SST	1987-1995	AVHRR	Brazil-Malvinas Confluence
Saraceno et al. 2005	SST CHL	1998-2003 1998-2003	AVHRR, AMSR-E SeaWiFS	Southwest Atlantic
Veitch et al. 2006	SST	1982-1999	AVHRR	Angola-Benguela Front
Wang et al. 2021	SST CHL	2004-2019 2007-2019	Multi-sensor MODIS	SW Atlantic
Wang et al. 2023	SST SSH	2010-2018 2010-2018	AVHRR Altimeters	SW Atlantic
Yu et al., 2015	SSS	2012-2013	Aquarius	Tropical Atlantic

Brazil Current/Front/Retroflection and Brazil-Malvinas Confluence: Among the most conspicuous thermal fronts in the World Ocean surveyed with early infrared satellite imagery, Legeckis (1978) emphasized the Brazil-Malvinas Confluence, a major water mass front between subtropical and subantarctic waters. Legeckis and Gordon (1982) reported intra-seasonal north-south migrations of the Brazil Current/Front. The advent of AVHRR in 1981 and subsequent implementation of the Pathfinder project (Minnett et al., 2019) stimulated studies of SST fronts, particularly in those areas where various physical processes create enhanced thermal contrasts between adjacent water masses. Such areas are mostly found in the coastal regions of the SW Atlantic and Eastern Atlantic. In the SW Atlantic, the Brazil Current/Front/Retroflection and Brazil-Malvinas Confluence were studied by Olson et al. (1988), Provost et al. (1996), Saraceno et al. (2004), Barré et al. (2006), Lorenzzetti et al. (2009), Artana et al. (2018), Artana et al. (2019), Castellanos et al. (2019), and da Silveira et al. (2023).

The Rio de la Plata plume features prominently in the salinity field. The Plata discharges over 22,000 m^3/s on average and up to 60,000 m^3/s at maximum (Guerrero et al., 1997; Piola et al., 2005; Acha et al., 2008; Campos et al., 2008). The Plata discharge is made of two major components, Paraná and Uruguay, that are anticorrelated; therefore, the seasonal variations of Plata discharge are relatively small, varying between 20,000 and 27,000 m^3/s according to Fig. 8 in Dogliotti et al. (2016) based on discharge data by Borús and Giacosa (2014). The first-ever synoptic aerial survey of the Plata Plume in winter 2003 documented the Plume's northward extent of 1100 km up to Itajaí (Brazil) at 27°S (Burrage et al., 2008). According to the modeling study by Piola et al. (2005), the Plata Plume extends north for up to 1300 km. In winter 1993, following an anomalously high Plata discharge, Plata water extended north by 1500 km up to 23°S (Campos et al., 1996; Campos et al., 1999; Campos et al., 2008). Analysis of historical precedents by Campos et al. (1999) showed that the penetration of Plata

 doi:10.20944/preprints202403.0975.v1

water into the South Brazil Bight is not an unusual event. The Plata water's northward penetration is driven largely by the wind stress rather than variations in the Plata discharge (Palma et al., 2008).

The Plata plume and associated fronts were studied, among others, by Guerrero et al. (1997), Garcia and Vargas (1998), Framiñan et al. (1999), Simionato et al. (2001), Möller et al. (2008), Moreira and Simionato (2019), and Lisboa et al. (2022), and were recently reviewed by Piola et al. (2018). The Plata Plume front is prominent in salinity, and it also manifests in SST in summer, when the Plata outflow is warmer than offshore waters (Guerrero et al., 1997, Fig. 6; Framiñan et al., 1999, Fig. 8.13). The collocated turbidity front was studied, among others, by Framiñan and Brown (1996), Dogliotti et al. (2016), and Maciel et al. (2021). The salinity front was studied from SMOS and Aquarius SSS data by Guerrero et al. (2014).

The Patos Lagoon outflow with average discharge of 2000 m^3/s (~10% of the Plata discharge) creates a plume that extends up to >30 km offshore across the inner shelf and >100 km alongshore, is bordered by a sharp salinity front with a cross-frontal step of 10 psu and is embedded in the Plata plume (Burrage et al., 2008).

The Patagonian Shelf features fronts of various nature (Acha et al., 2004; Rivas and Pisoni, 2010; Piola et al., 2018; Brun et al., 2020), including tidal mixing fronts (Glorioso, 1987), especially in the Gulf of San Jorge (Palma et al., 2020) and off Península Valdés. The Patagonian Shelf is bordered by the **Shelf-Break Front** (Franco et al., 2008; Combes and Matano, 2018; Franco et al., 2022).

The Subtropical Shelf Front was identified first from in situ data by Piola et al. (2000), who also studied this front from satellite data (Piola et al., 2008b). Cross-shelf oceanographic sections by Muelbert et al. (2008) revealed a strong two-step ("double") thermohaline front in winter (T=12-18°C, S=33.0-36.5), when this TS-front extended vertically from the sea surface to the shelf break, whereas in summer this front manifested in salinity only (S=33.7-35.2).

Surface thermal fronts of the SW Atlantic were studied from satellite SST data by Saraceno et al. (2005), Rivas (2010), Rivas and Pisoni (2010), Bouali et al. (2017), Wang et al. (2021), and Wang et al. (2023).

Magellan Plume: The surface salinity field of the southern Patagonian Shelf is strongly affected by the inflow of low salinity water from the Magellan Strait, Le Maire Strait and along the Cape Horn shelf break (Palma and Matano, 2012; Brun et al., 2020; Guihou et al., 2020). Brun et al. (2020, Fig. 2) presented an up-to-date climatological map of salinity at 20 m depth over the Patagonian Shelf from in situ data. This map shows the freshwater outflow from the Magellan Strait extending north up to 43°S. This flow transports up to 0.074 Sv, thereby providing "a strong interoceanic connectivity associated with diluted subantarctic waters of the Pacific Ocean through the Magellan Strait which in turn are further diluted largely by inflows from the Almirantazgo Fjord via the Whiteside Channel. … The low salinity inflow from the Magellan Strait combines with saltier inflows through the Le Maire Strait and farther east that feed the Atlantic shelf." (*ibid.*, p.1).

The Congo River outflow with long-term (2000-2010) annual mean discharge of 40,662 m^3/s (Alsdorf et al., 2016) creates a huge freshwater plume, whose space-time variability and dynamics have been extensively studied (Denamiel et al., 2013; Hopkins et al., 2013; Reul et al., 2014; Vic et al., 2014; Chao et al., 2015; Sorí et al., 2017; Munzimi et al., 2019; Phillipson and Toumi, 2019; Laraque et al., 2020; Houndegnonto et al., 2021; Martins and Stammer, 2022; Jarugula and McPhaden, 2023; Wongchuig et al., 2023). Similar to other river plumes, the Congo River plume could feature *fronts* in SST and SSS that could either bound the plume or could be embedded in the plume; however, this aspect of the Congo River outflow remained unexplored to date. Chao et al. (2015) studied offshore freshwater anomalies created by variations in the Congo River outflow in 2011-2013. When the Congo River discharge quadrupled between August 2012 and January 2013, this caused an offshore low-salinity anomaly (observed along Aquarius orbital tracks some 400 km from the river mouth) that peaked in February 2013, about a month after the discharge peak of >60,000 m^3/s in January 2013 (*ibid.*, Fig. 5 and Fig. 9).

The main water mass front in Eastern Atlantic is **the Angola-Benguela Front (ABF)** at the confluence of the warm southward Angola Current and the cold northward Benguela Current (Shannon et al., 1987; Meeuwis and Lutjeharms, 1990; Lass et al., 2000; Mohrholz et al., 2004; Veitch

 doi:10.20944/preprints202403.0975.v1

et al., 2006; Vizy et al., 2018). This quasi-zonal front migrates in the general north-south direction on the seasonal and interannual time scales, spanning a wide range of latitudes and including multiple fronts, thus called the Angola-Benguela Frontal Zone.

Another prominent frontal zone in the SE Atlantic is associated with the **Benguela Upwelling** (Andrews and Hutchings, 1980; Lutjeharms and Meeuwis, 1987; Hutchings et al., 2009). The upwelling gives rise to upwelling fronts, particularly in the southern Benguela, between Cape Agulhas (35°S) and Cape Columbine (33°S) (Hutchings et al., 1986; Armstrong et al., 1987). The **Benguela Upwelling Frontal Zone** (e.g., Belkin et al., 2009) consists of two isolated frontal zones separated at the Lüderitz line (27°S). This separation is independently documented by Duncombe Rae (2005) and is collocated with the area of high winds and low chlorophyll at 26-27°S pointed out by Hutchings et al. (2009). This separation is also nearly collocated with a sharp bathymetric change at about 28°S, where the broad shelf to the south contrasts with the narrow shelf to the north. In addition to a strong negative signal in SST, the Benguela upwelling manifests as a negative signal in SSS (up to −0.6 psu), which is documented, among others, by Muller et al. (2013) and Hösen et al. (2016), the latter providing statistics on 450 upwelling filaments that extend up to >500 km offshore.

Compared to coastal fronts, **the open-ocean fronts** attracted less attention. Belkin (1993) analyzed sparse historical data to distinguish the North and South STF some 400-500 km apart, thus forming the **Subtropical Frontal Zone (STFZ)** extending quasi-zonally at 35-40°S. This double-front pattern was confirmed, among others, by Belkin and Gordon (1996) and Smythe-Wright et al. (1998) and is consistent with the double-front pattern of STF presented by Lutjeharms et al. (1993). In the central South Atlantic, Juliano and Alves (2007) documented a major zonal current/front at 34-35°S and termed it the **St. Helena Current/Front** after the St. Helena high pressure system centered over St. Helena Island at 20°S. Vianna and Menezes (2011) noted this geographic incongruence and termed this jet the **Tristan da Cunha Current** after the Tristan da Cunha Islands at 37°S. Burls and Reason (2006) studied SST fronts between 25°S and 55°S. Funke (2009) used satellite data to study the STF in the central South Atlantic. Billany et al. (2010) studied fronts at the Greenwich Meridian. Dencausse et al. (2011) studied the STFZ in the SE Atlantic. Bouali et al. (2017) estimated 12-year trends of SST gradients (fronts) in the entire South Atlantic. The **Subantarctic Front (SAF)** observed at 45-50°S in numerous in situ studies has never been comprehensively studied from satellite data (save for the Meeuwis (1991) PhD study) as opposed to the **Polar Front (PF)**, which has been a subject of several remote sensing studies. In this regard, Peterson and Stramma (1991, p.47) noted: "The course of the SAF has been studied to a much lesser extent than that of the PF, which is partly because the SAF is not always clear in the surface temperature fields; it is better identified with upper-layer salinities." The Polar Front was mapped by Moore et al. (1997), Moore et al. (1999), Trathan et al. (1997), Dong et al. (2006), and Freeman and Lovenduski (2016).

2. Data and Methods

SSS Data: We used SSS data from SMOS (Kerr et al., 2010; Reul et al., 2014; Boutin et al., 2018; Reul et al., 2020; Boutin et al., 2021; Boutin et al., 2023). We used *high-resolution* SMOS SSS data provided by the Barcelona Expert Center (BEC; smos-bec@icm.csic.es), where nine years (2011-2019) of SMOS data were reprocessed and daily global SSS maps generated as documented by Olmedo et al. (2021). We used BEC Level 4 SMOS SSS daily data with horizontal resolution of 0.05°× 0.05° or approximately 5.6 km × 5.6 km at the equator. These data were downloaded from https://bec.icm.csic.es/bec-ftp-service/.

Front detection: We used the Belkin and O'Reilly (2009) algorithm (BOA) to calculate horizontal gradients of SSS. High-gradient zones are identified with salinity fronts. The BOA is widely used thanks to its efficiency and simplicity (Belkin, 2021). The BOA uses a contextual shape-preserving, scale-sensitive, adaptive median filter that effectively eliminates impulse/shotgun/salt-and-pepper noise. At the same time, the BOA does not smooth ramp-like steps (fronts). It also retains intact roof-like ridges and significant peaks or valley-like minima (local pointwise freshening events). The BOA's median filter can be applied iteratively. The iterative median filter, when applied to a one-dimensional dataset (e.g., a time series), is known to converge to a root signal (Gallagher and Wise,

 doi:10.20944/preprints202403.0975.v1

1981). However, when applied to a 2D dataset (e.g., an image), the iterative median filter does not necessarily converge. Our experiments with the BOA's iterative MF confirmed the lack of convergence while processing daily mean global SMOS SSS fields. The main reason for that is probably the overall smoothness of BEC L4 data. Therefore, after the first 10-15-20 iterations, when the MF removes remaining noise, the subsequent iterations do not result in any improvement. Therefore, the number of iterations can be kept at a minimum.

Logarithmic transformation of data: Logarithmic transformation (or log-transform) of experimental and remote sensing data has a long history (Irons and Petersen, 1981; Currant-Everett, 2018). A typical situation when log-transform is needed is when experimental data distribution is highly skewed. When data distributions are far from normal, statistical tests developed for normally distributed data cannot be applied. Also, highly skewed 2D data are difficult to visualize, especially when the data range spans a few orders of magnitude, which is a common situation in digital image processing (Gonzalez and Woods, 2018; Gonzalez et al., 2020), including digital processing of satellite imagery.

Log-transform in satellite oceanography: In oceanography, following the seminal work by Campbell (1995), the log-transform has been routinely applied to CHL data, particularly to global CHL data provided by satellites because (1) the global distribution of original CHL data is highly skewed, and (2) the global CHL data range is wide (Gregg and Casey, 2004; Werdell et al., 2018). Other oceanic remotely sensed observables are almost never transformed since the observed data do not span orders of magnitude, especially in the open ocean, and also because their distributions are not highly skewed. The above does not apply to some derived quantities, e.g., gradients. For example, Zhang et al. (2014) have log-transformed gradient magnitude (GM) of SST data from the Taiwan Strait and demonstrated the lognormality of GM data.

Log-transform of SSS: To bring out SSS fronts, we ran the BOA algorithm (Belkin and O'Reilly, 2009) over SSS data to obtain salinity gradients. Maps of gradient magnitude GM of SSS reveal zones of enhanced GM that are salinity fronts. The frequency distribution of GM is strongly skewed; therefore, we log-transformed GM using natural logarithms (ln). The frequency distribution of log-transformed gradient ln(GM(SSS)) is symmetrical and fairly normal, while maps of log-transformed gradient presented in the next section reveal more features, particularly fronts. Using the terminology of digital image processing, the log-transform enhances contrasts across digital maps (Gonzalez and Woods, 2018; Gonzalez et al., 2020).

3. Results

3.1. Large-Scale Open-Ocean Salinity Fronts

Large-scale pattern of sea surface salinity:

The large-scale (ocean-wide) pattern of SSS is fairly stable year-round as evidenced by long-term (2011-2019) mean monthly maps of SSS that feature low-salinity equatorial belt, high-salinity subtropical pool, and general salinity decrease due south toward 45-50°S (Figure 1a (January-June) and Figure 1b (July-December)).

 doi:10.20944/preprints202403.0975.v1

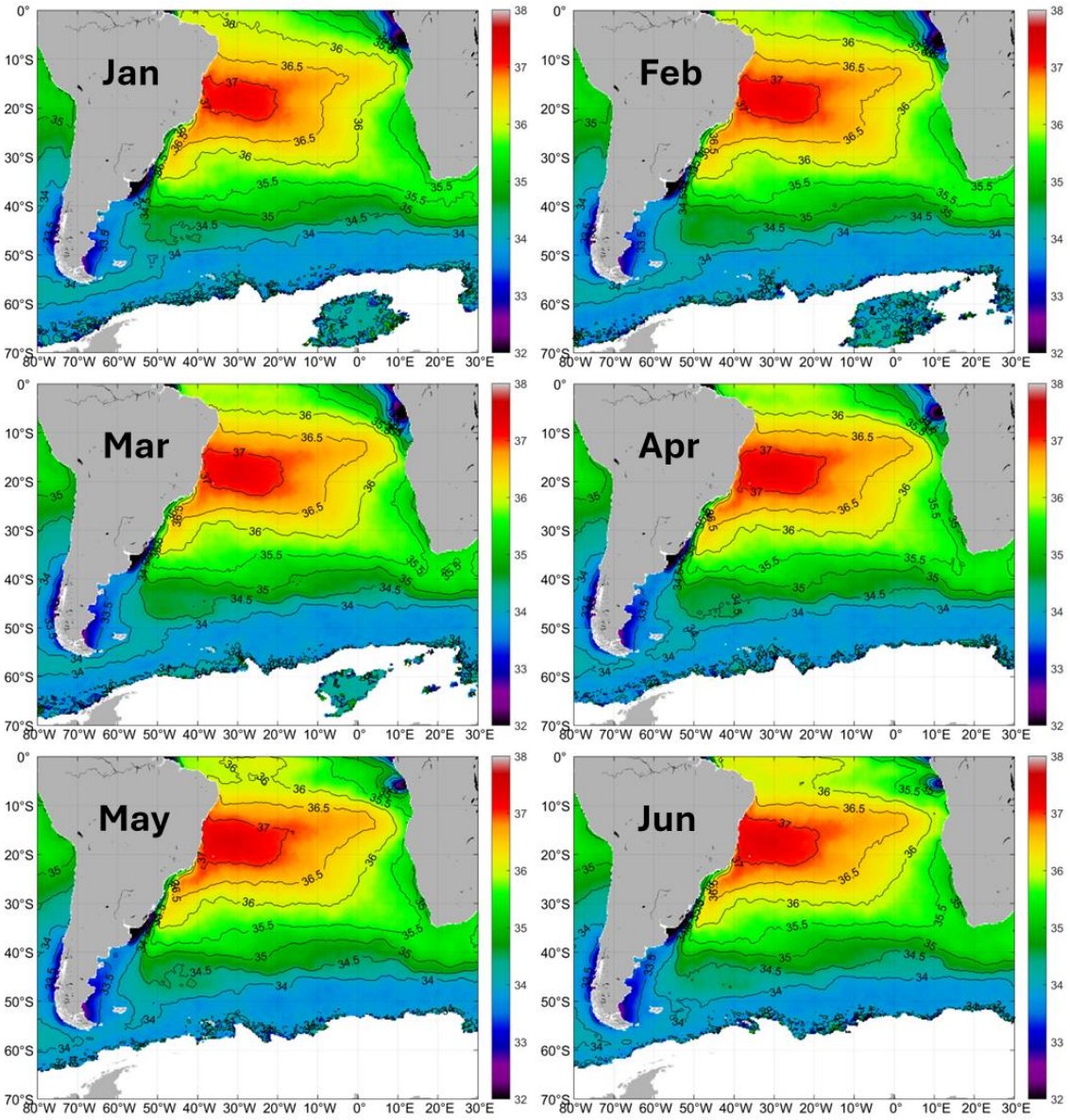

(**a**)

 doi:10.20944/preprints202403.0975.v1

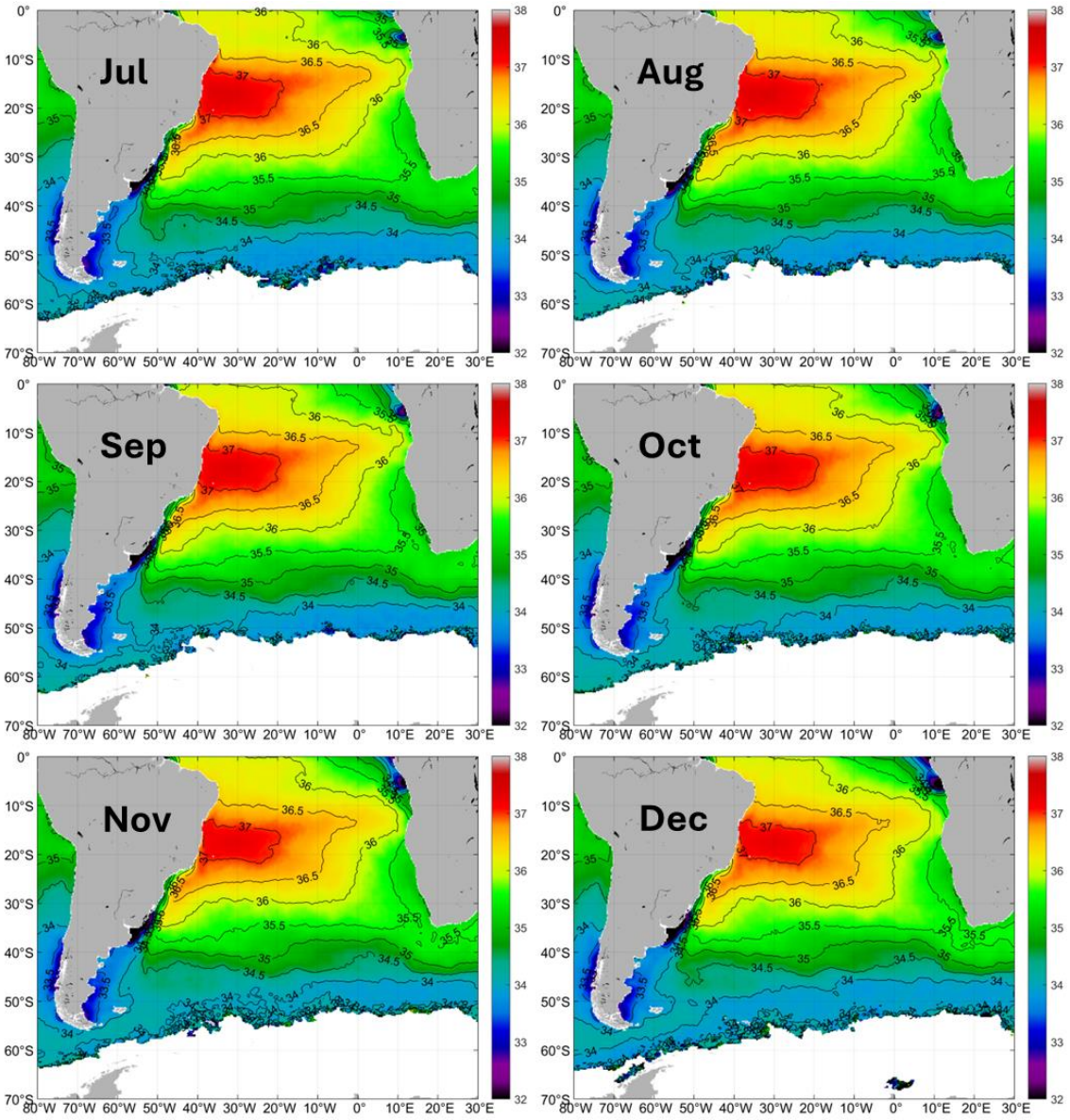

(**b**)

Figure 1. a. Long-term (2011-2019) mean monthly maps of SSS. January-June. **b.** Long-term (2011-2019) mean monthly maps of SSS. July-December.

Superimposed on this ocean-scale pattern, there are four large-to-mesoscale regions of low-salinity: (1) Rio de Plata region (RP); (2) Magellan Strait region (MS); (3) Congo River region (CR), and (4) Benguela upwelling region (BU). The ocean-wide maps of SSS do not reveal visually apparent zones of high horizontal gradients of SSS (salinity fronts) except for salinity fronts that border the outflows of two great rivers, Rio de la Plata and Congo. The large-scale open-ocean pattern of SSS does not qualitatively change seasonally or interannually. Unlike the large-scale open-ocean fronts that remain fairly stable seasonally and interannually, the above-mentioned four large-to-mesoscale regions off the coasts of South America and Africa experience substantial seasonal variability reported below and also experience occasional interannual fluctuations caused by global events like El Niño.

Salinity fronts: An overview

Salinity fronts become apparent after running the BOA algorithm that calculates gradients of SSS (Figure 2a,b) The following large-scale open-ocean quasi-zonal fronts can be distinguished in all monthly maps, north to south: (1) Tropical Front (TF) between 15-20°S; (2) Western Subtropical Front (WSTF) near 30°S; (3) Eastern Subtropical Front (ESTF) near 35°S; (4) Subantarctic Front (SAF) near

 doi:10.20944/preprints202403.0975.v1

45°S; and (5) Polar Front (PF) near 50°S (close to 60°S in the Drake Passage). In addition to these high-gradient zones (fronts), we detected a quasi-zonal narrow belt of zero gradient (which corresponds to the absolute salinity maximum) that crosses the Tropical Atlantic south of the Tropical Front.

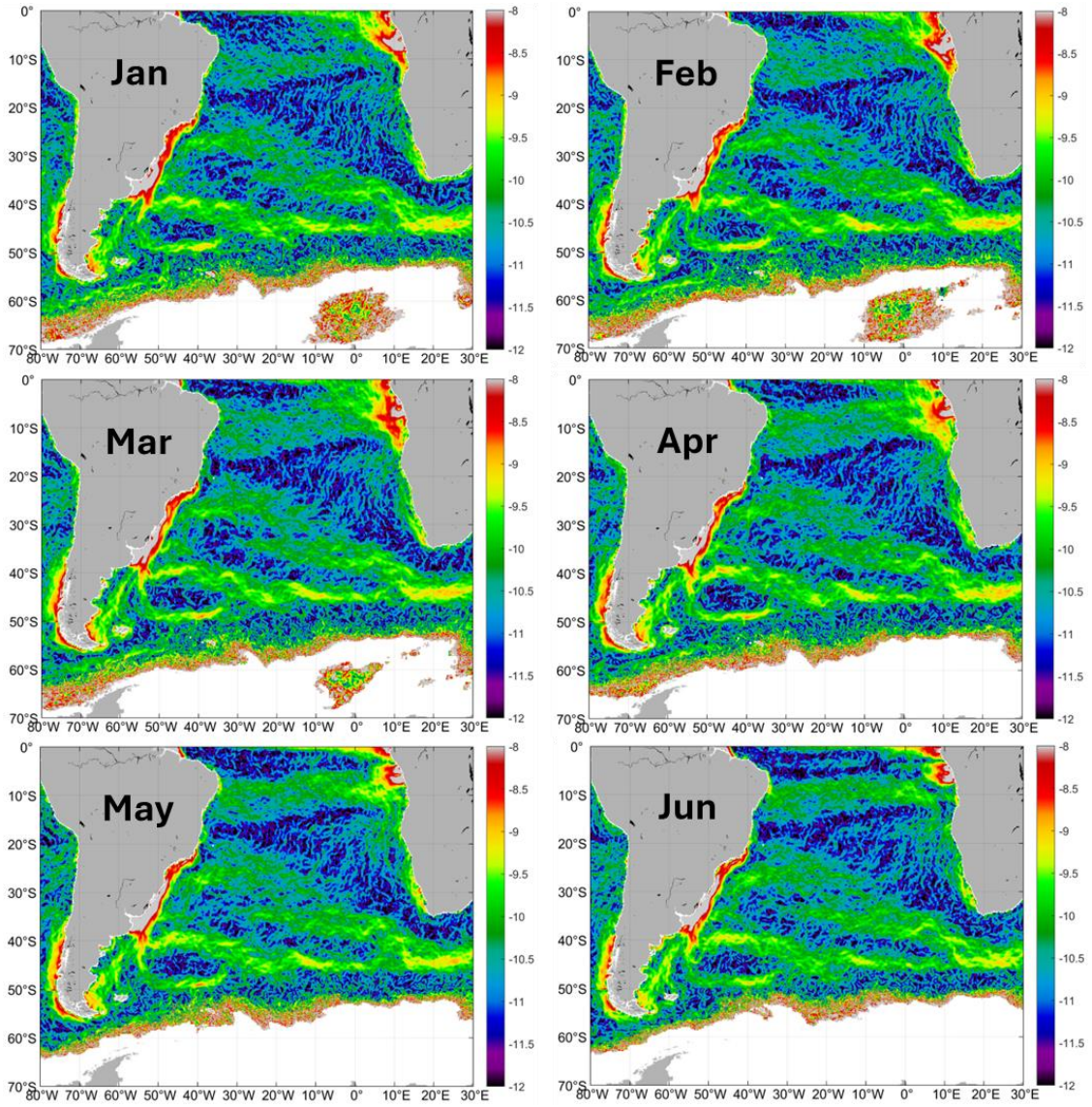

(**a**)

 doi:10.20944/preprints202403.0975.v1

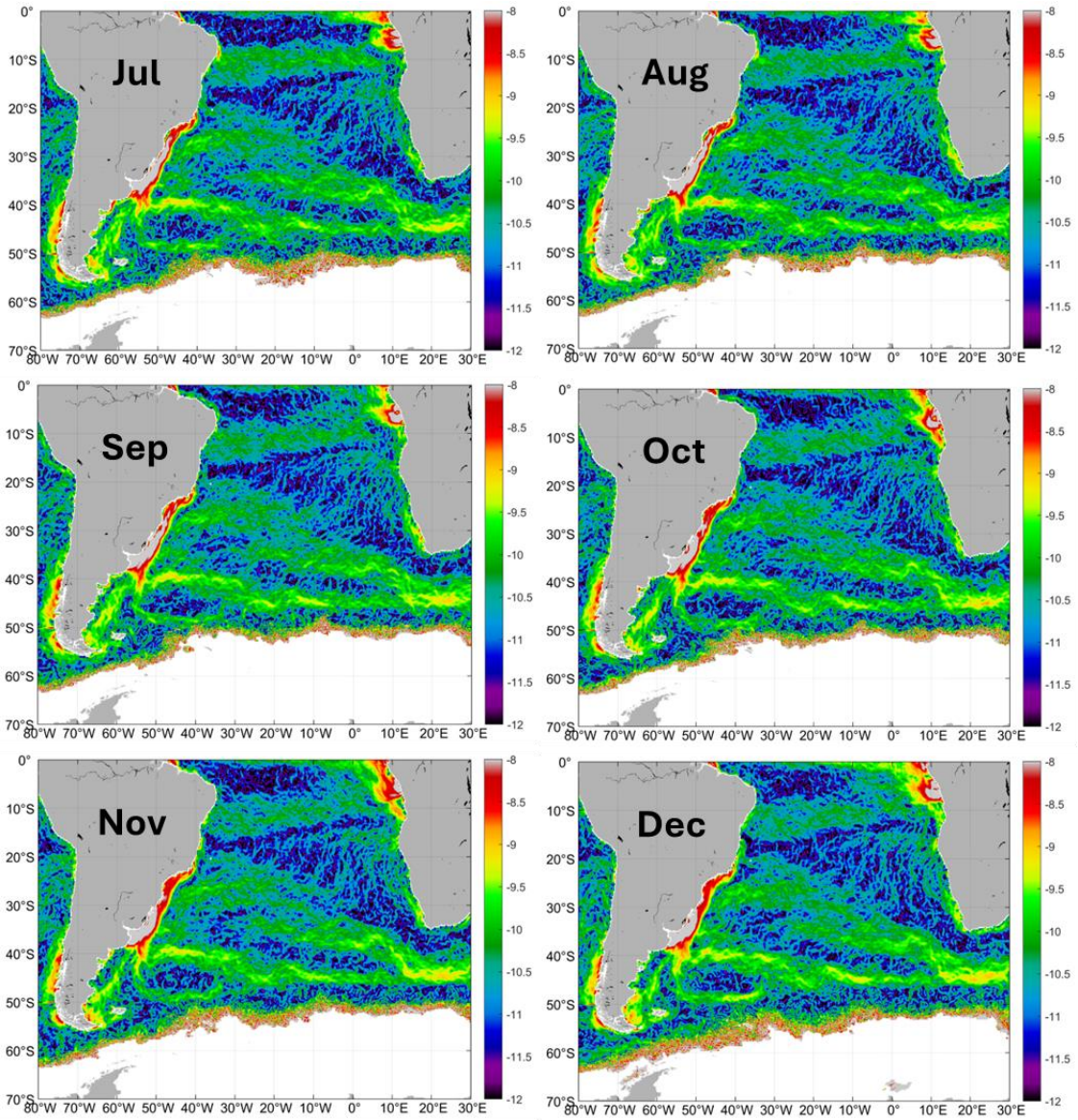

(**b**)

Figure 2. a. Log-transformed gradient magnitude GM of sea surface salinity SSS. January-June. **b.** Log-transformed gradient magnitude GM of sea surface salinity SSS. July-December.

Meridional (north-south) and zonal (west-east) variations of surface salinity:

Since the above-mentioned large-scale fronts are quasi-zonal, their main characteristics (intensity and strength) are best determined along meridians that cross the fronts quasi-normally. We chose 14 meridians spaced 5° of longitude apart, from 45°W to 20°E. Distributions of SSS vs. latitude along every 10° of longitude are shown in Figure 3.

 doi:10.20944/preprints202403.0975.v1

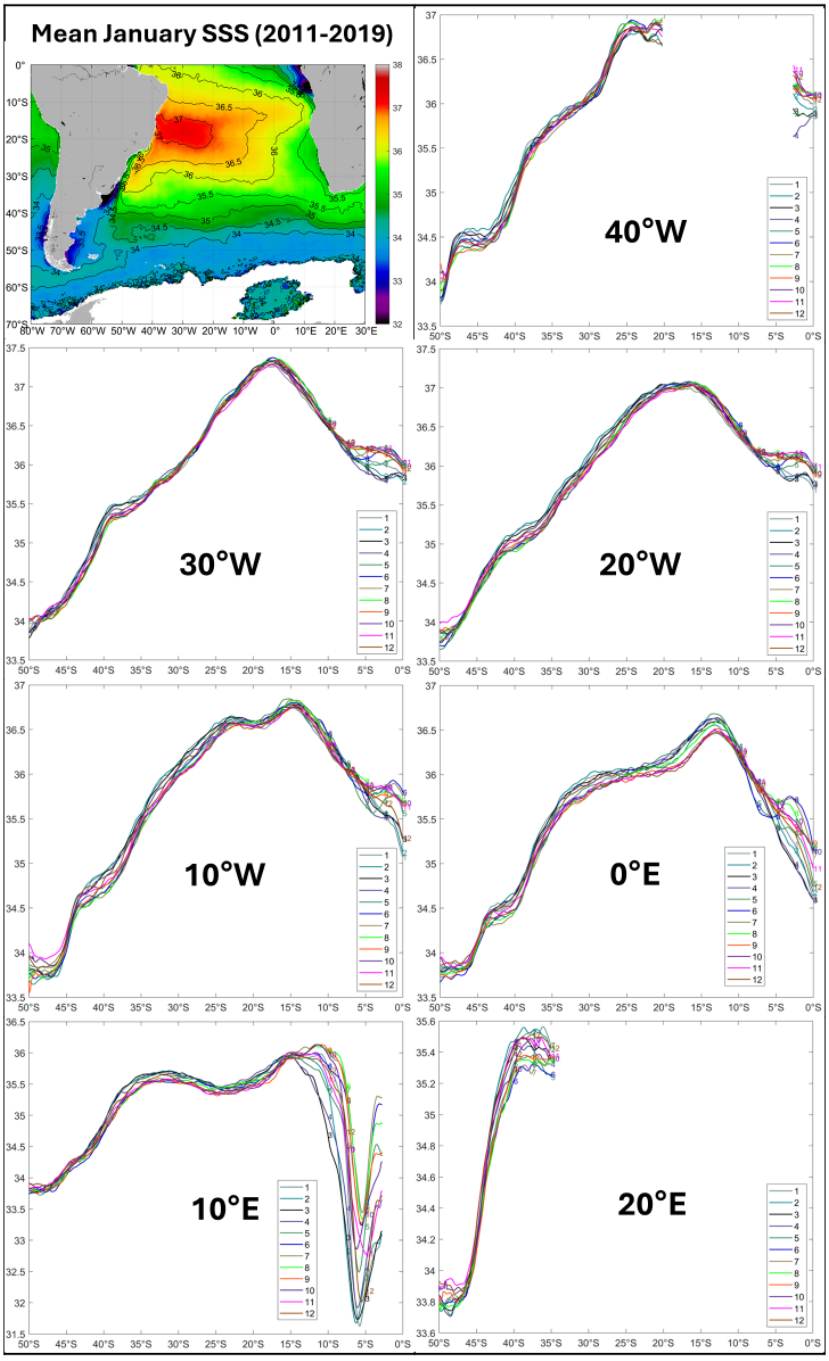

Figure 3. Long-term (2011-2019) mean monthly distributions of SSS along 7 meridians between 40°W-20°E from the equator to 50°S. Monthly curves are numbered as in the legend (1, Jan, … 12, Dec).

Each subplot shows 12 long-term (2011-2019) mean monthly distributions of SSS vs. latitude along a given meridian, illustrating the year-round stability of the meridional (north-south) pattern of SSS except for the equatorial belt and Congo River outflow. Similar meridional distributions of SSS vs. latitude for individual years, 2011 through 2019 (not shown), illustrate the interannual stability of the meridional (north-south) pattern of SSS except for the equatorial belt and Congo River outflow. The seasonal and interannual stability of the meridional (north-south) distributions of SSS contrasts sharply with the relatively strong zonal (west-east) variations of the meridional distributions of SSS. Indeed, substantial qualitative (morphological) changes of the meridional distributions of SSS occur between meridians just 5° of longitude apart that is <500 km at 30°S. Thus, the large-scale meridional pattern of SSS experiences qualitative changes in the west-east direction at the upper mesoscale (500 km).

 doi:10.20944/preprints202403.0975.v1

Large-scale pattern of open-ocean salinity fronts:

The large-scale open-ocean salinity fronts appear as broad zones of enhanced gradient that are several hundred kilometers wide (Figures 1–3). The apparent breadth of salinity fronts can be partly accounted for by the original spatial resolution of SMOS data (35-50 km). It cannot be accounted for by temporal averaging of daily SMOS data used in this study as evidenced by sample comparisons of daily, monthly, annual, and multi-annual (2011-2019) mean meridional (north-south) distributions of SSS. Owing to the temporal stability of large-scale open-ocean salinity fronts, these fronts retain their main characteristics such as width and gradient after temporal averaging on monthly, annual, and multi-annual scales. The rather smooth large-scale appearance of meridional distributions of SSS is not unusual as it has been observed elsewhere, e.g., in the North Atlantic (Kolodziejczyk et al., 2015).

Tropical Front:

A close inspection of monthly gradient maps (Figure 2) reveals (1) seasonal migrations of the Tropical Front in the north-south direction and (2) seasonal variations in spatial orientation of this front. The north-south range of seasonal migration is rather small, about 2° of latitude. The front's spatial orientation ("tilt") varies seasonally in sync with the front's north-south seasonal migrations. When the front reaches its northernmost location, its orientation is strictly zonal. When the front reaches its southernmost location, its non-zonal orientation (tilt) is at maximum.

Salinity Maximum:

Immediately south of the Tropical Front, a narrow quasi-zonal band of zero salinity gradient, which corresponds to the salinity maximum (Smax), crosses the Tropical Atlantic between 15-20°S. Obviously, the high-salinity subtropical pool must feature salinity maximum somewhere inside the pool. However, the well-defined persistent linear morphology of the Smax belt was unexpected and has not been reported before. The Smax belt shifts north-south seasonally in sync with the north-south shifts of the Tropical Front. The Smax belt orientation (tilt) varies in sync with that of the Tropical Front. The persistence of the Smax belt, which shifts north-south seasonally while retaining its well-defined linear morphology, is suggestive of a mechanism that maintains this feature.

Subtropical Frontal Zone (STFZ):

The West Subtropical Front (WSTF) is well defined in the western part of the South Atlantic, where it extends quasi-zonally along 30°S. **The East Subtropical Front (ESTF)** is well defined in the eastern part of the South Atlantic, where it extends quasi-zonally along 35°S.

Subantarctic Front (SAF) and Polar Front (PF):

The SAF extends quasi-zonally southeast and east of the Brazil-Malvinas Confluence along 45-48°S. The PF is located south of the SAF along 48-50°S. The SAF and PF appear merged between 30°W and 45°W where both fronts extend along the northern flank of the Falkland Ridge. This is the same area where the SAF-PF merger was documented from in situ data by Peterson and Whitworth (1989).

Meso-scale quasi-meridional tropical-subtropical fronts:

Gradient maps (Figure 3) reveal an enigmatic ripple pattern of multiple quasi-meridional fronts extending between the Tropical Front and East Subtropical Front. This pattern covers a vast triangular area in the Tropical/Subtropical Atlantic, where the ripple field stretches due west from Africa toward Brazil. Within this ~2000-km-long area, ~20 fronts are regularly spaced ~100 km apart. The ripple pattern evolves seasonally, being best defined during the boreal winter, e.g. in January. Similar mesoscale streaky fronts can be seen elsewhere, e.g., in the SW Atlantic. However, the eastern tropical-subtropical ripple field stands out owing to its sheer size and regular structure.

3.2. Rio De La Plata Outflow

Monthly maps of SSS (Figure 4a,b) and SSS gradient magnitude (Figure 5) reveal seasonal variations of the Rio de la Plata (RP) estuarine front and seasonal alongshore migration of the RP plume. The estuarine front extends northward along the coast of Uruguay and Brazil in winter, reaching its maximum extent typically in June-July (except for October-November in 2015). In 2019 the Plata plume reached its maximum northern extent in June and persisted off the SE Brazil for five months through October. The large extent and longevity of the Plata plume in winter 2019 was caused

 doi:10.20944/preprints202403.0975.v1

by the extremely high Plata discharge, which in turn was caused by the record-high discharge of Uruguay River, which for a few days exceeded the Parana River discharge, albeit normally the former is about 1/3 of the latter (Aubriot et al., 2020; Kruk et al., 2021).

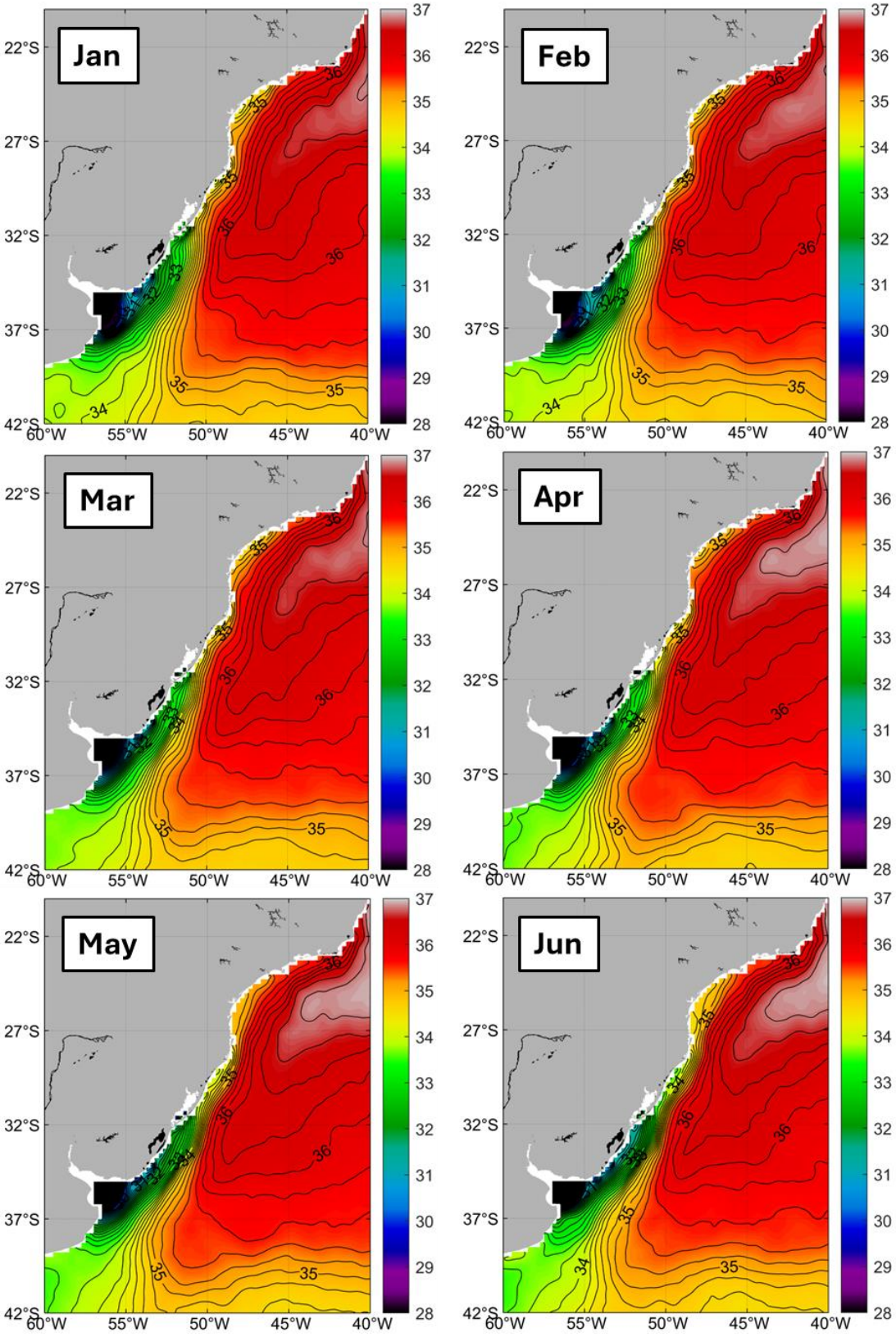

(**a**)

 doi:10.20944/preprints202403.0975.v1

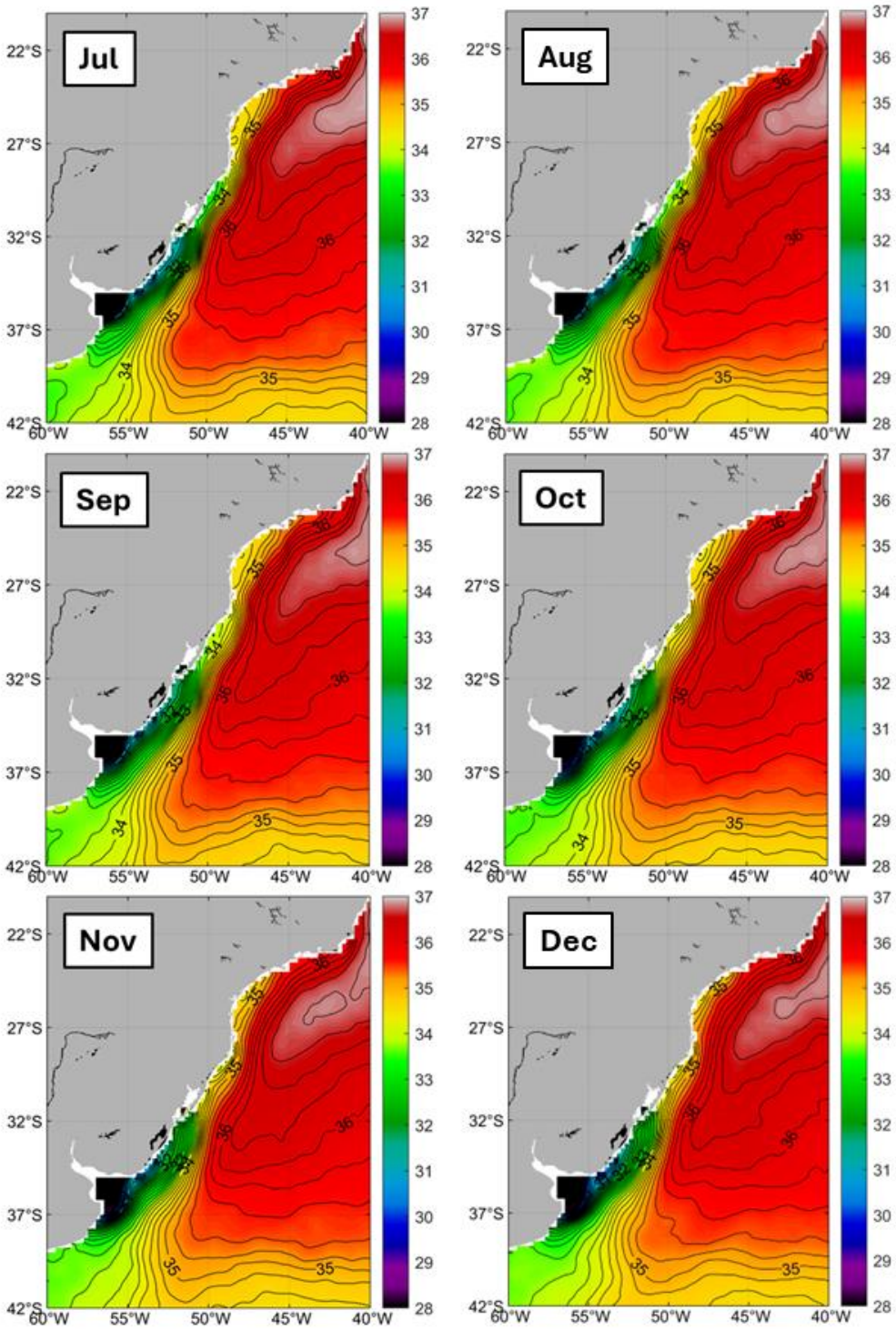

(**b**)

Figure 4. a. Long-term (2011-2019) mean monthly SSS in the Rio de la Plata outflow region. January-June. **b.** Long-term (2011-2019) mean monthly SSS in the Rio de la Plata outflow region. July-December.

 doi:10.20944/preprints202403.0975.v1

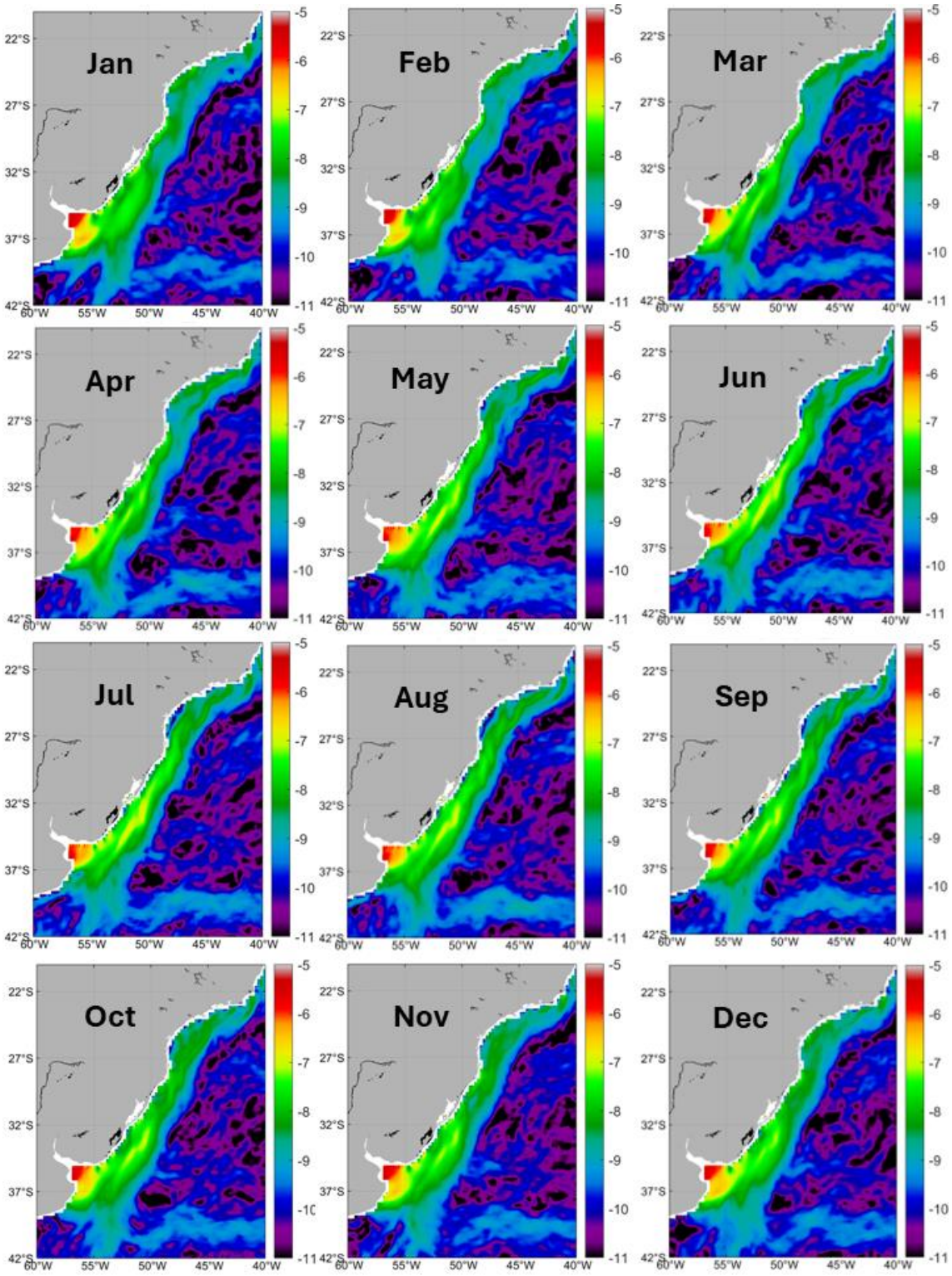

Figure 5. Long-term (2011-2019) mean monthly log-transformed gradient of SSS in the Rio de la Plata outflow region.

The alongshore northward propagation of the RP plume is facilitated by the persistent wintertime southerly winds. The alongshore progress of the RP plume can be traced by using the 31.0 isohaline off Uruguay or the 34.0 isohaline off the SE Brazil or the 35.0 isohaline into the South Brazilian Bight. Piola and Romero (2004) used the 33.5 isohaline to trace the diluted Plata waters.

The northernmost extent of the Plata water in the South Brazilian Bight (23-28°S) is more difficult to determine unambiguously because of freshwater discharges by numerous rivers that empty into

 doi:10.20944/preprints202403.0975.v1

the Bight (Marta-Almeida et al., 2021). Nonetheless, the Plata water may extend due north up to 23°S (~1500 km from the Plata estuary) during El Niño winter seasons (Campos et al., 1996).

The Plata plume's extension to the south along the coast of Argentina is quite limited year around and varies very little seasonally and interannually. The plume's front can be identified with the 33.4-33.6 isohalines (Figure 6), which is consistent with the 33.5 isohaline used by Piola and Romero (2004) to track the plume's extension to the north. The preferred direction of the Plata plume spreading to the north is confirmed by numerical models. Monthly maps of SSS gradient magnitude GM (Figure 7) show that the GM peaks in the Samborombón Bay (off the coast of Argentina) year-round. This is consistent with the results obtained by Framiñan and Brown (1996) from a multiyear statistical analysis of SST imagery. Our finding is interesting because the majority of studies postulate the northern route (along the coast of Uruguay) to be the dominant pathway for the Plata water spreading offshore. The southern route via the Samborombón Bay is widely considered to be minor vs. the northern route. However, the idea of the southern flow being slow and the Samborombón Bay being almost stagnant is incompatible with the year-round presence of enhanced salinity gradients as evidenced by the SMOS data.

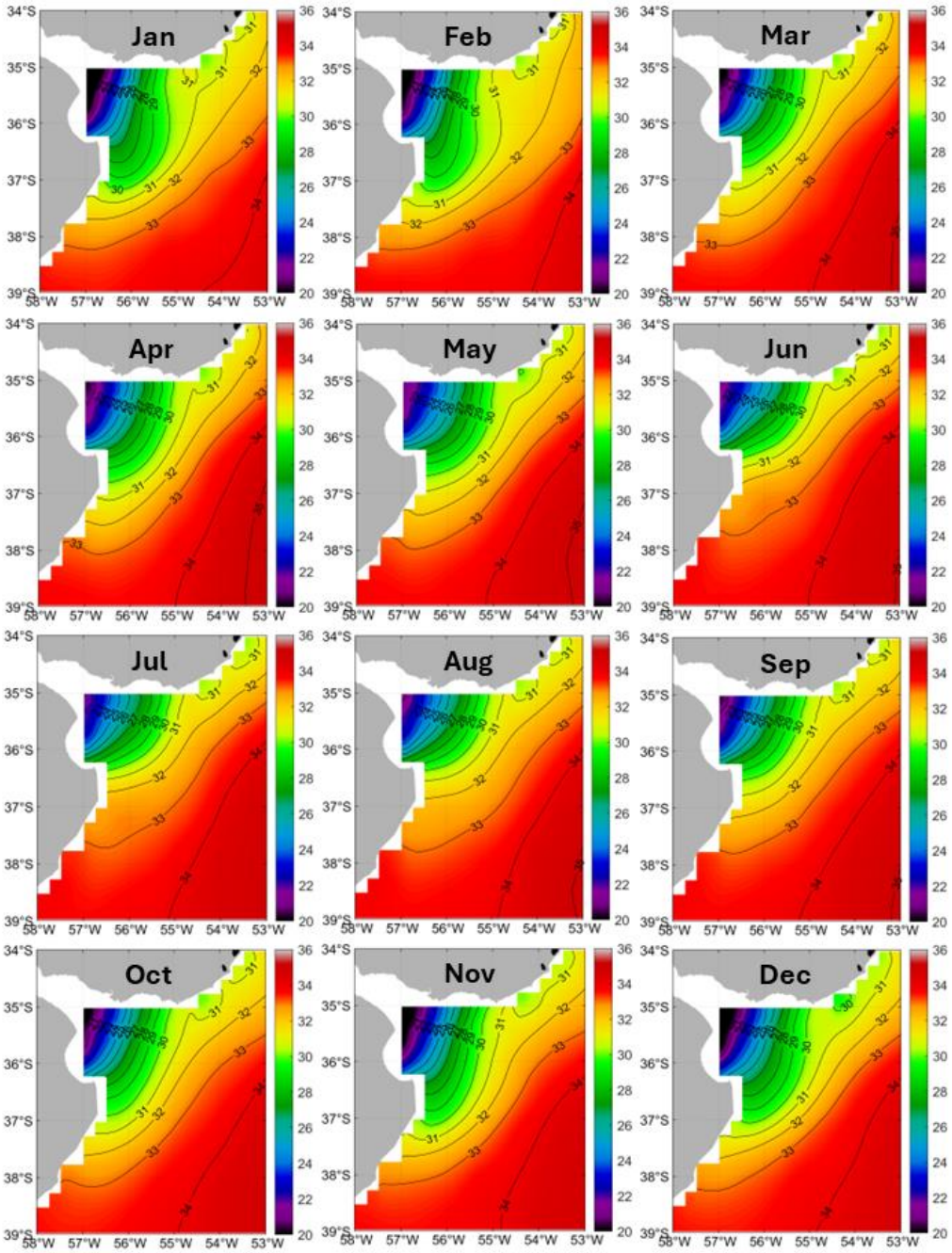

 doi:10.20944/preprints202403.0975.v1

Figure 6. Long-term (2011-2019) mean monthly maps of SSS in the Plata Estuary region.

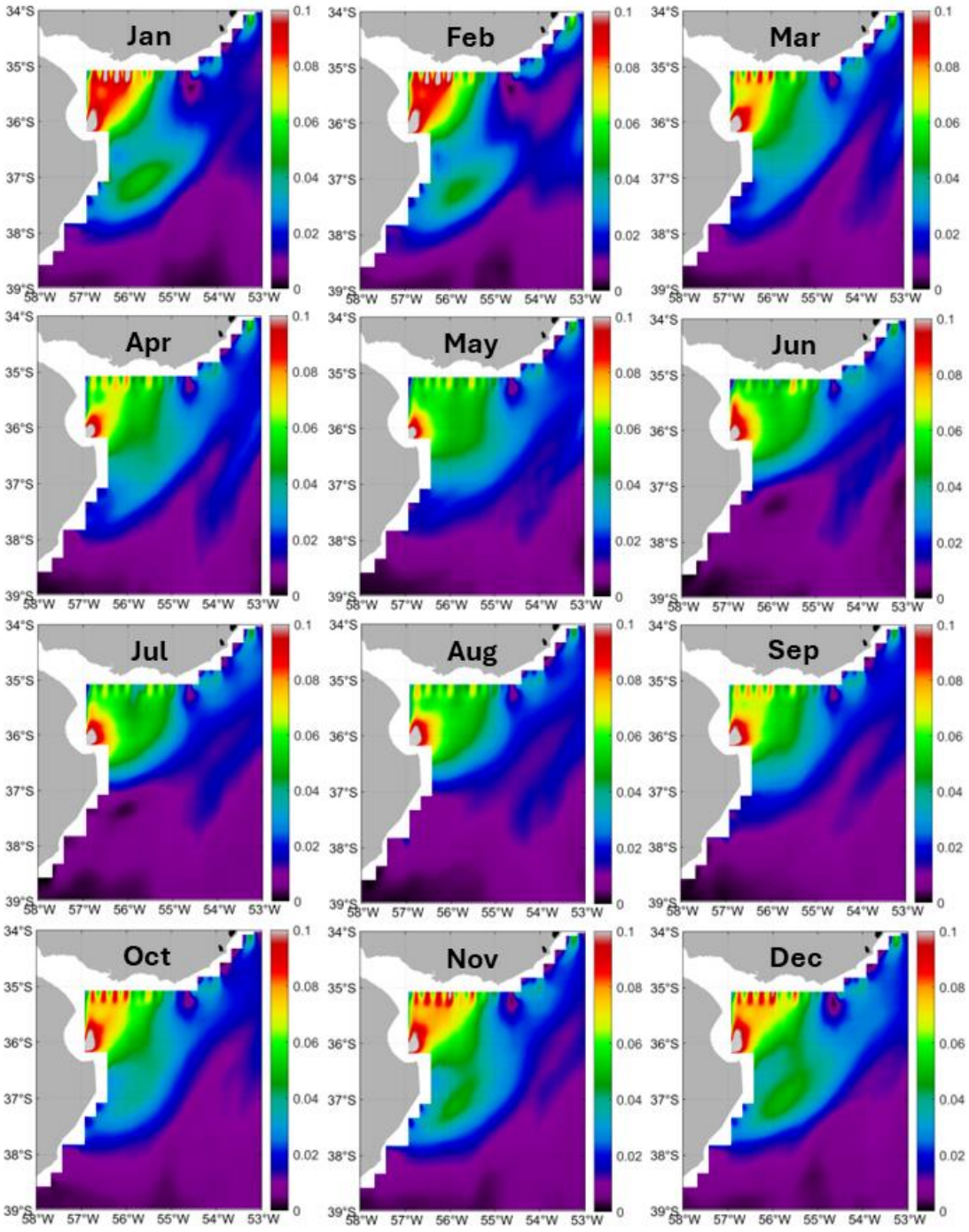

Figure 7. Long-term (2011-2019) mean monthly maps of log-transformed gradient of SSS in the Plata Estuary region.

The low-salinity outflow from the Patos Lagoon is barely noticeable in the monthly maps of SSS (Figure 4) and SSS gradient magnitude (Figure 5), including such maps for individual months (not shown). According to the detailed aerial mapping by Burrage et al. (2008), the size of the outflow bulge was 33 km x 100 km with SSS inside the bulge varying between 12 and 27 psu, ranging by ~10 psu from 18 to 28 psu across a well-defined bulge front. Given the 5-km resolution of the SMOS data used in this study, the detection of the Patos Lagoon outflow is possible in principle.

 doi:10.20944/preprints202403.0975.v1

The Plata estuarine front is identified with the 30.0 isohaline (Figure 6). As the season progresses, this front expands offshore in October-January and retreats inshore in February-June to stay along the Barra del Indio shoal till September. The front also changes its orientation as its western end (off the coast of Argentina) shifts from ~36°S in June to ~37°S in January, while its eastern end (off the coast of Uruguay) remains stationary year-round at ~34.5°S.

The low-salinity coastal belt's northern limit can be defined by the 34.0 isohaline, which migrates seasonally from 31.5°S in summer (November-April) to 28.5°S in winter (May-September). An alternative (broader) definition of the low-salinity coastal belt would use the 36.5 isohaline as the belt's northern boundary, which marks an interface between the low-S coastal belt and high-S subtropical gyre. The interface is not smooth. Instead, the interface is collocated with a sharp along-shore gradient of SSS (Figure 5). The low-S coastal tongue extends throughout the South Brazil Bight (SBB) year-round up to Cabo Frio (23°S, 42°W) and beyond, reaching 21°S in December-January (Figure 4). This conclusion is consistent with the climatological surface salinity map presented by Piola et al. (2018, Fig. 1a) and based on an extensive collection of in situ data. Most studies of the SBB oceanography invoke local rivers' discharge to explain the low salinity (<34.0) of coastal waters. With the total discharge of local rivers into the SBB exceeding 4,000 m^3/s (Marta-Almeida et al., 2021), their impact cannot be ignored. A modeling study of river plumes in the SBB by Marta-Almeida et al. (2021) revealed a low-salinity nearshore tongue propagating along the coast throughout most of the SBB up to 25.5°S and possibly occasionally up to Cabo Frio at 23°S, 42°W.

3.3. Magellan Strait and Le Maire Strait Outflows

The **Magellan Strait region** in this study extends to Cape Horn (56°S, 67°W). The spatial and seasonal variability of SSS and SSS fronts in this region are illustrated by sample maps for mid-summer and mid-winter (Figure 8). The SSS field of the southern Patagonian Shelf is strongly affected by the outflow of low-salinity water from the Magellan Strait. This outflow has two sources. One is the Pacific Ocean off Western Patagonia. Another is the copious amount of local precipitation onto the Magellan Strait watershed. The low-salinity Pacific water also flows to the Eastern Patagonian Shelf along the Western Patagonia shelf break, where it is carried south and east by the Cape Horn Current (Brun et al., 2020). After bypassing Cape Horn, the Pacific water enters the Patagonian Shelf via Le Maire Strait (Brun et al., 2020). Lagrangian simulations by Guihou et al. (2020) inferred a net NE-ward transport of 0.88 Sv across 51°S.

 doi:10.20944/preprints202403.0975.v1

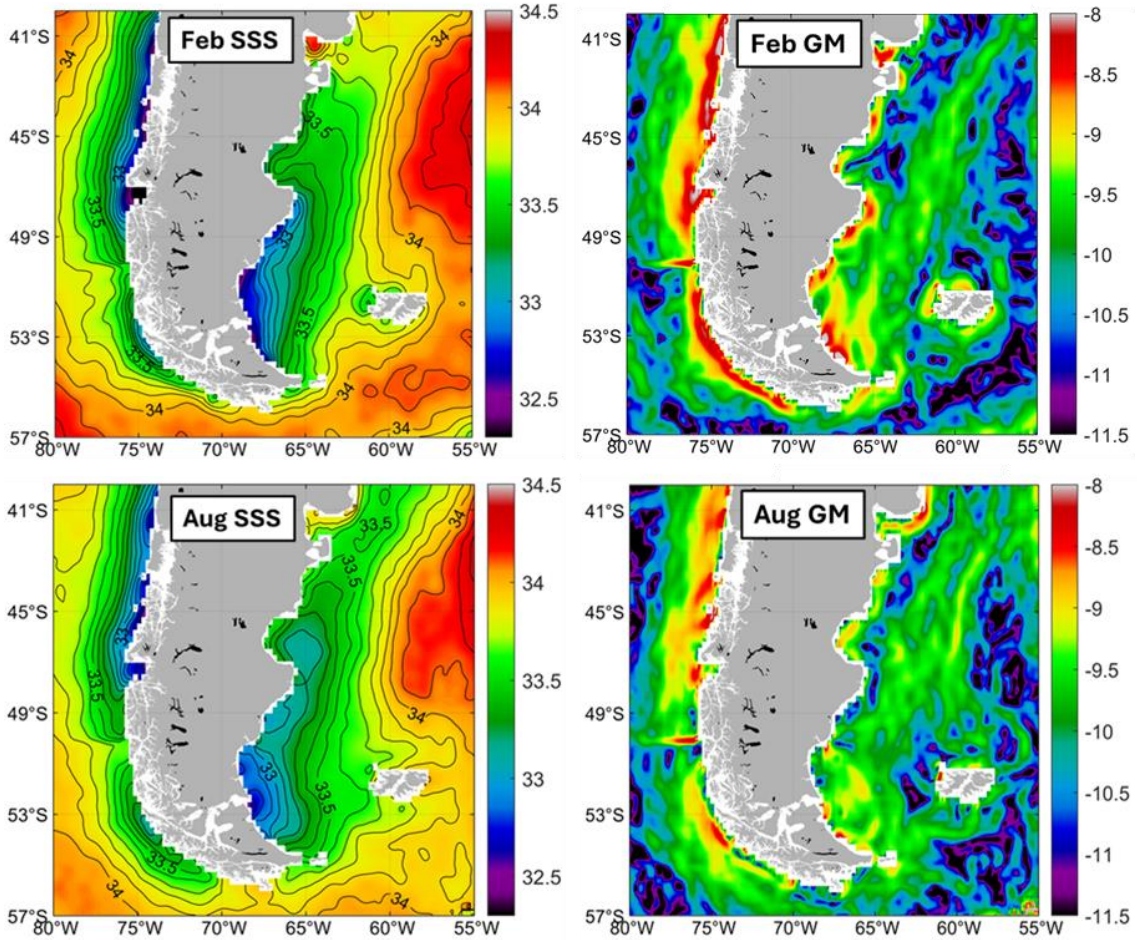

Figure 8. Long-term (2011-2019) mean monthly maps of SSS and log-transformed gradient magnitude (GM) of SSS in mid-summer (February) and mid-winter (August) in the Magellan Strait outflow region.

Brun et al. (2020, Fig. 2) presented an up-to-date climatological map of salinity at 20 m depth over the Patagonian Shelf from in situ data. This map shows the freshwater outflow from the Magellan Strait extending north up to 43°S (see the map). The SMOS data lend itself to improve this picture. According to the SMOS data, the low-salinity Magellan Strait water (S<33.5) extends to 44°S in winter (June-July) and up to 40°S in late spring and summer (November-January). A close inspection of 108 individual monthly maps of SSS in 2011-2019 shows that the MS water occasionally extends north beyond 40°S where it merges with the Rio de la Plata outflow. The MS outflow is bounded by a well-defined front at some distance east of the eastern entrance to the strait. This front does not appear to be terribly robust as the MS plume extends north along the coast of Eastern Patagonia. In that respect the MS plume qualitatively differs from the Rio de la Plata plume. Our maps do not resolve the individual flows that emanate from the Magellan Strait and Le Maire Strait. The low salinity tongue formed by the combined flow extends north alongshore driven by the northerlies. According to Piola et al. (2018), the combined low-salinity tongue eventually merges with the Rio de la Plata plume. Our maps support this conclusion. The combined low-salinity tongue forms a relatively low-intensity salinity front at its interface with ambient waters.

The low-salinity outflow from the Magellan Strait (MS) exhibits seasonal variations in its spatial extent. The MS plume's boundary can be identified with the 33.5 psu isohaline (as, e.g., in Palma and Matano, 2012), which is the same isohaline that is commonly used to delineate the Plata plume. The MS plume (defined by the 33.5 isohaline) extends north along the Patagonian coast from the Magellan Strait's eastern entrance off Punta Dungeness (52°24'S, 68°26'W) up to 40°S in winter (June-July) but

 doi:10.20944/preprints202403.0975.v1

only to 44°S in spring-summer (November-January). The MS outflow is fed by a pool of low-salinity waters off western Patagonia (40°S-55°S), which is split into two parts, with a gap in-between at ~50°S (Davila et al., 2002). It's the southern part of the low-salinity belt that feeds the MS throughflow.

The MS plume's characteristics (salinity, area, and northward extent) largely depend on (1) the amount, timing, and salinity of the low-salinity Pacific water coming down the Strait; (2) amount and timing of the MS watershed precipitation; (3) wind stress field over the Eastern Patagonian Shelf. The vast pool of low-salinity water off Western Patagonia south of 35°S is created by copious amounts of precipitation falling on the western slopes the Chilean Andes. This vast freshwater pool consists of two parts (lobes) separated by a wedge of more saline water at 50°S (Dávila et al., 2002). The SMOS SSS data allowed us to document this feature in detail. The monthly maps of SSS and SSS fronts (Figure 8) revealed a sharp SSS front at 50°S, which is the southern boundary of the northern lobe of low salinity and the northern edge of the gap between the northern and southern lobes of low salinity. The gap remained absolutely stable during the 9-year study period, showing no signs of either seasonal or interannual variability. Bathymetry is deemed to be the only reason for such uncanny stability of an ocean feature. The northern lobe waxes and wanes seasonally, apparently in accordance with seasonal variations of precipitation. Using the 33.7 psu isohaline to delineate the northern lobe, its area peaks in December when the 33.7 isohaline extends west beyond 80°W. Since the northern lobe is separated from the southern lobe of low salinity, it is not clear whether the low salinity water from the north can be transported to the western entrance of the Magellan Strait. The southern lobe's seasonal variations are out of sync with the northern lobe. Indeed, the southern lobe's area peaks in March-May and shrinks in October-January. Salinities of both lobes are quite different, with the southern lobe being much saltier than the northern lobe. Moreover, the southern lobe's minimum salinity is much higher than the minimum salinity of the Magellan Strait outflow. If the southern lobe contributes significantly to the MS outflow, the southern lobe's salinity must be substantially diluted by local precipitation within the Magellan Strait watershed, which is extremely high.

3.4. Congo River Outflow

The Congo River Plume waxes and wanes as the season progresses as evidenced by the monthly maps of SSS and SSS gradient (Figures 9 and 10). The Plume's spatial extent and minimum axial SSS vary in sync. The Plume grows in October-March and shrinks in April-September. During the Plume's maximum extent in January-February, its axial minimum SSS (immediately offshore the river mouth) drops down to ~30 psu. During the Plume's minimum extent in July, its axial minimum SSS is ~32 psu.

 doi:10.20944/preprints202403.0975.v1

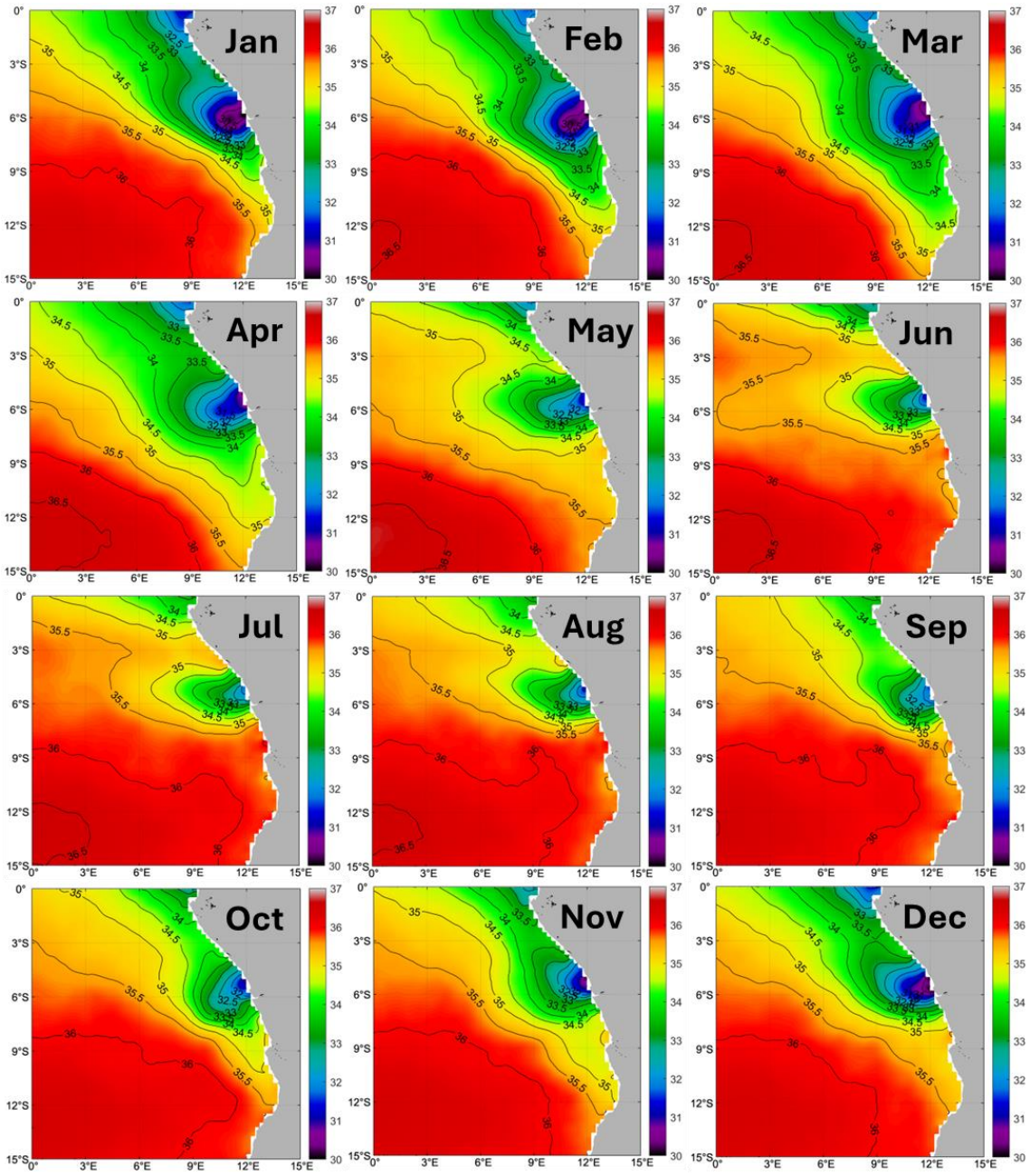

Figure 9. Long-term (2011-2019) mean monthly maps of SSS in the Congo River outflow region.

 doi:10.20944/preprints202403.0975.v1

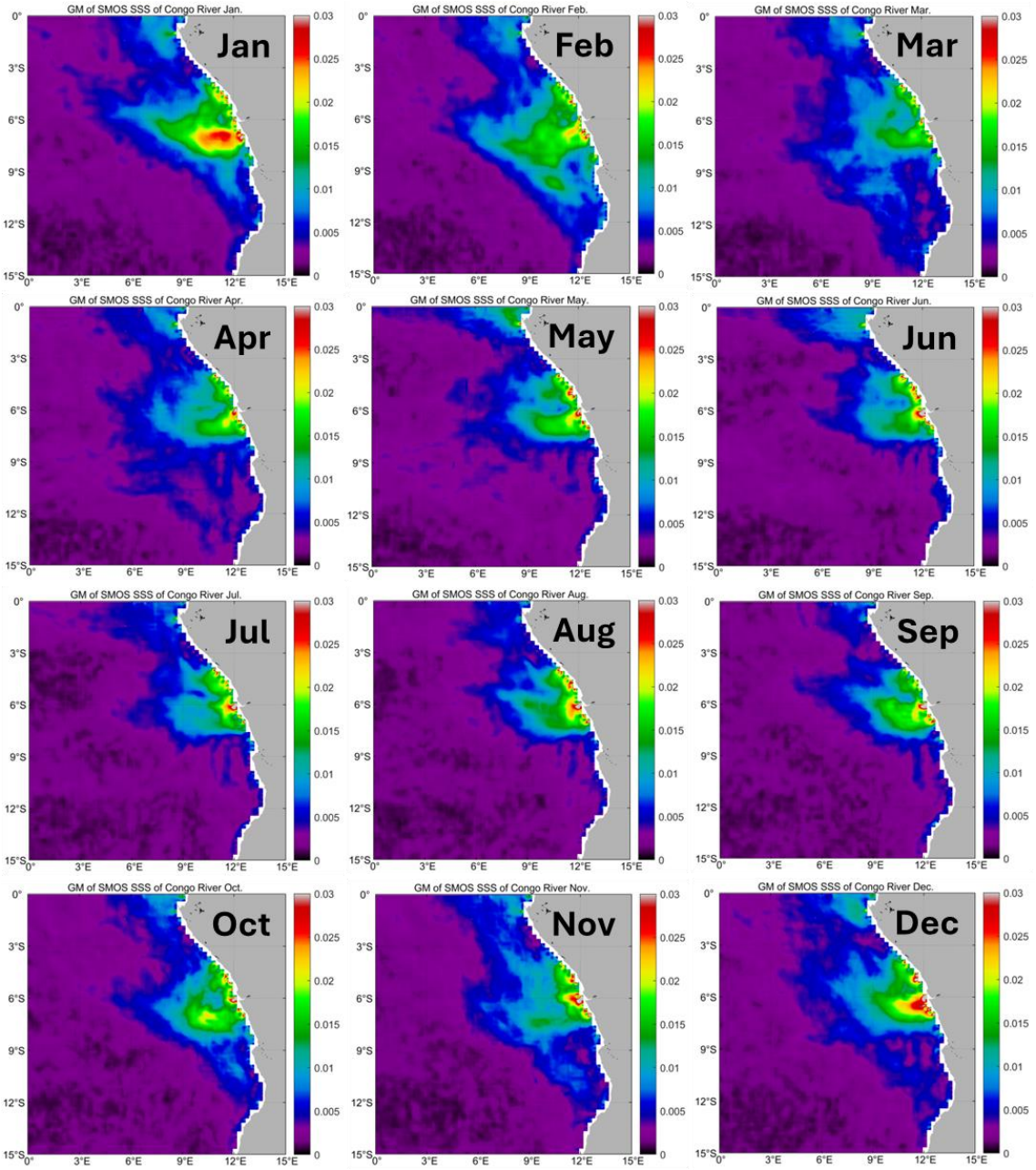

Figure 10. Long-term (2011-2019) mean monthly maps of log-transformed gradient magnitude (GM) of SSS in the Congo River outflow region.

The Plume Front exhibits a dominant mode of spatial orientation, which is a quasi-zonal extension to the west along 6°S as evidenced by monthly maps of salinity gradient (Figure 10). The meridional plots of SSS along 10°E (Figure 3) document the seasonal stability of this locational mode, which varies within 1° of latitude between 5°S and 6°S. The local bathymetry south of the Congo River Canyon does not provide any clue to the front's stability. The Plume Front's spatial stability contrasts with the substantial seasonal variability of the Plume Front's intensity and strength that correlate with the Plume's seasonal variations in extent and minimum salinity noted above.

The monthly maps of SSS (Figure 9) reveal seasonal and interannual variability of the Congo River outflow and its spreading off shore and alongshore. The Congo River discharge (CRD) has its main peak in summer (January-February). The CRD's main peak translates without much delay into the seasonal growth and spreading of the Plume, whose extent peaks in January-February. The absence of a significant delay is not surprising given the extremely swift outflow, up to 2.5 m/s at the

 doi:10.20944/preprints202403.0975.v1

mouth. Since the Kinshasa-Brazzaville gauges are located about 500 km upstream of the mouth, the time lag between the gauges and mouth is about 500000/2.5=200,000 s /86400 s/day < 3 days.

The monthly maps of SSS gradient (Figure 10) reveal the CR plume front (CRPF) and make evident the significant seasonal variability of the front's morphology, extent, location, and orientation. The outflow direction varies widely from NW alongshore to westward offshore to SE alongshore. The plume morphology and extent can be estimated objectively with a proper algorithm, which would be outside the scope of this study. Nonetheless, the modal location and orientation of the Plume front are apparent from monthly maps of SSS gradient (Figure 10): Most often, the plume front extends quasi-zonally along 6°S. This is the first known determination of the modal location and orientation of the Plume front. Admittedly, this result is not quite rigorous; an objective method is needed to delineate the front and quantify its movements, orientation, and morphology.

3.5. Angola-Benguela Front

The ABF is a quasi-zonal front, extending west from the African coast for a few hundred km along 16°S and migrating north-south seasonally and interannually. The ABF is a strong temperature front and also a structural front bordering from the south the sharp and shallow tropical thermocline. In the salinity field the ABF is weak with a cross-frontal range of mere 0.2-0.3 psu, typically spread over a few hundred km, thus never forming a sharp salinity front. Occasionally, the ABF lacks any manifestation in the salinity field, at least in the surface layer. The monthly maps of SSS and SSS gradient in the Congo-Angola-Benguela region (Figure 11) do not show any sign of enhanced SSS gradient within the zonal band of the thermal ABF (15-17°S) or immediately south of it.

Preprints.org (www.preprints.org) | NOT PEER-REVIEWED | Posted: 18 March 2024 doi:10.20944/preprints202403.0975.v1

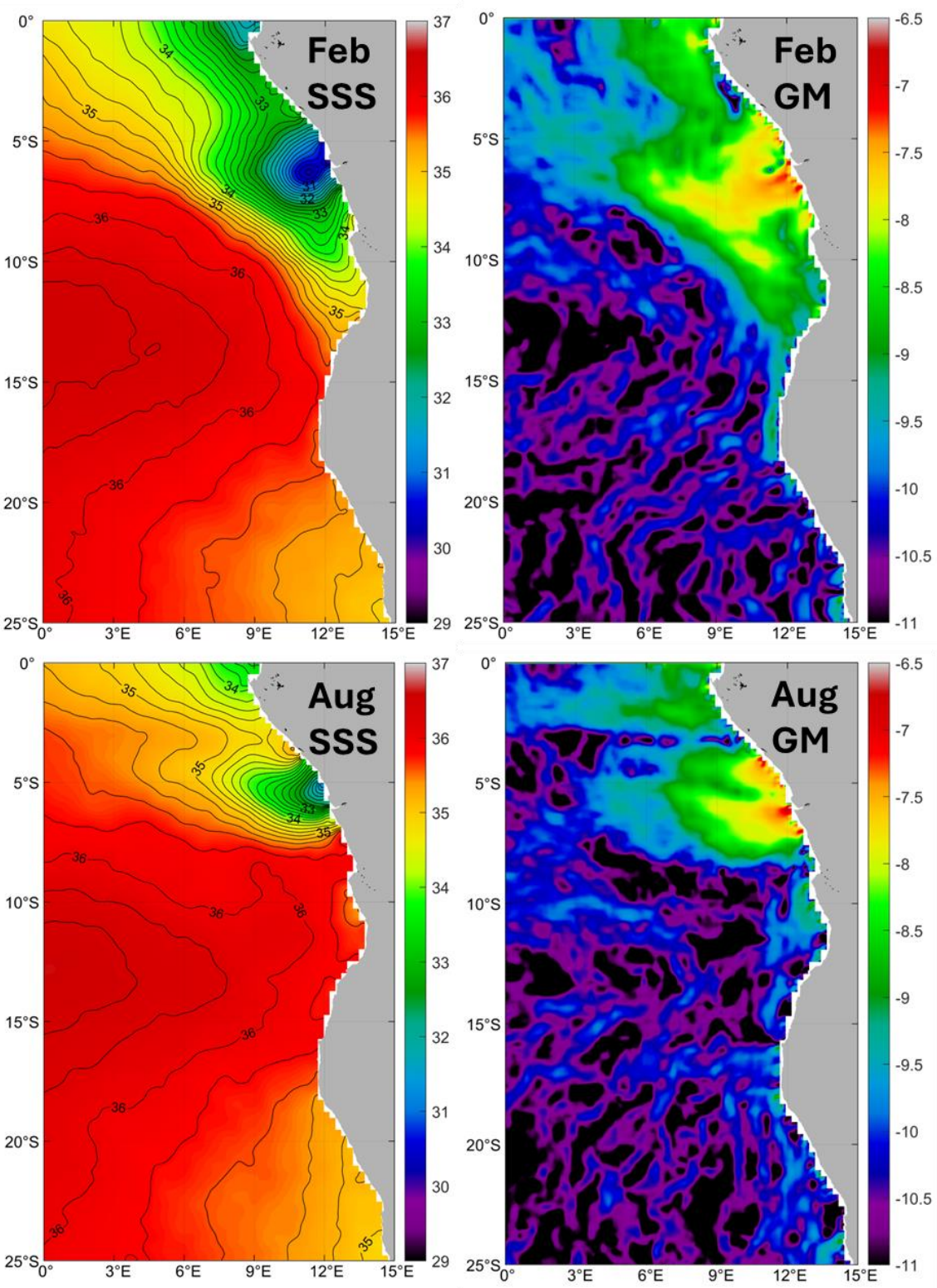

Figure 11. Long-term (2011-2019) mean monthly maps of SSS and log-transformed gradient magnitude (GM) of SSS in mid-summer (February) and mid-winter (August) in the Congo-Angola-Benguela region.

The most striking result is the absence of the Angola-Benguela Front (ABF) in the SSS and SSS gradient (Figure 11) fields. South of the tropical maximum of SSS, across a broad latitudinal range between 10°S and 25°S and farther south in the SE Atlantic, the offshore SSS decreases southward in a very gradual fashion. This general north-south decreasing trend in SSS reflects a large-scale transition from tropical waters to subtropical waters. This transition manifests in the SST field as a

 doi:10.20944/preprints202403.0975.v1

strong thermal front (with a total cross-frontal SST range of up to 6°C and a well-defined local maximum of SST gradient), which can be quite sharp at times. Surprisingly, unlike the great majority of ocean fronts, this thermal front is not accompanied by a local horizontal maximum in the SSS gradient field (Figure 11), a defining characteristic of a salinity front. In the SST field, the ABF manifests as a well-defined gradient maximum between 15.5°S and 17°S (Veitch et al., 2006).

There is much less certainty, if any, regarding the ABF manifestation in the salinity field, especially in the surface layer, where the ABF presence is tenuous at best despite some evidence to the contrary. In the seminal paper on the ABF, Shannon et al. (1987, p.11) wrote: "Although salinity data suggest that the front may extend to a depth of at least 200 m, it is particularly marked in the upper 50 m where it can be defined in terms of both temperature and salinity" yet noted "the salinity "front" (which is admittedly weakly defined)" (*ibid.*, p.19). The alongshore salinity data in Shannon et al. (1987, Fig.7) reveal a week salinity front at 17-18°S with a cross-frontal step of 0.2-0.3 psu, from 35.3-35.4 in the south to 35.6 in the north.

The April-May 1997 CTD survey of the ABF by R/V Petr Kottsov (Lass et al., 2000) revealed a strong SST front, with SST ranging from 25°C at 14°S to 16°C at 17°S, while SSS gradually decreased from 36.2 at 14°S to 35.6 at 17°S and decreased farther south at the same rate (*ibid.*, Fig. 5). Thus, there was no enhanced north-south gradient of SSS – hence no SSS front – within a broad, strong SST front. Similarly, the February-March 2002 CTD survey of the ABF by FRS Africana (Ekau and Verheye, 2005) documented a strong SST front, from 26°C at 16°S to 19°C at 18°S, with no attendant SSS front, albeit a strong SSS front was found much farther south at 20°S (*ibid.*, Fig. 1).

The absence of SSS front can be explained by influx of fresh water from the Gulf of Guinea, with the Congo River discharge (CRD) deemed to be the main constituent. The idea of the CRD (originated at ~6°S) affecting the ABF at 16°S – thus >1000 km away – might appear far-fetched to some researchers. For example, the CRD impact was not even mentioned by Shannon et al. (1987). Nonetheless, this idea of CRD-ABF link seems to have been established by now. The CRD's impact can be quite dramatic during Benguela Niños as, e.g., in 1995 when the negative SSS anomaly reached -4 psu in Angolan waters (Gammelsrød et al., 1998).

The classical concept of the Angola Current carrying warm and saline tropical waters has been augmented by Mohrholz et al. (2004, pp.1337-1339): "The Angola Current transported in its surface part less saline water from the great rivers in the north towards the ABFZ. … Along the continental slope the Angola Current advected warm and less saline surface waters (originating from the great rivers in the Gulf of Guinea) to 13°S, and warm tropical waters to 19°S." Thus, the influx of warm and fresh water from the Gulf of Guinea does not attenuate the thermal signature of the ABF yet greatly reduces the salinity contrast across the ABF, which explains the absence of SSS front within the ABF latitudinal range (15-18°S) in our results (Figures 9–11).

3.6. Benguela Upwelling Front

The dominant persistent southeasterlies blowing along the west coast of South Africa drive year-round coastal wind-induced upwelling in a vast region – Benguela upwelling (BU) -- between Cape Agulhas at 35°S and Cape Frio at 18°S. The cold upwelled water stands out in SST maps that have been extensively used in numerous studies of the BU's temporal and spatial variability. Salinity data have not been systematically utilized to date. The SMOS data clearly portray the BU region of low salinity and document its seasonal variability (Figure 12). The BU region includes several upwelling cells, each bordered by a local front. The entire BU region is bordered by a front called the Benguela Upwelling Front (BUF) by von Bodungen et al. (2008). The BUF is well defined in the upper 20-40-m layer as, e.g., in May 2004, when R/V Alexander von Humboldt's zonal transect T3 along 17°S crossed the unperturbed BUF normally with SST=17-20°C and SSS=35.6-35.9 (von Bodungen et al., 2008, Fig.6). The monthly maps of SSS gradient magnitude GM (Figure 12) reveal either a single salinity front or numerous salinity fronts that comprise the BUF.

 doi:10.20944/preprints202403.0975.v1

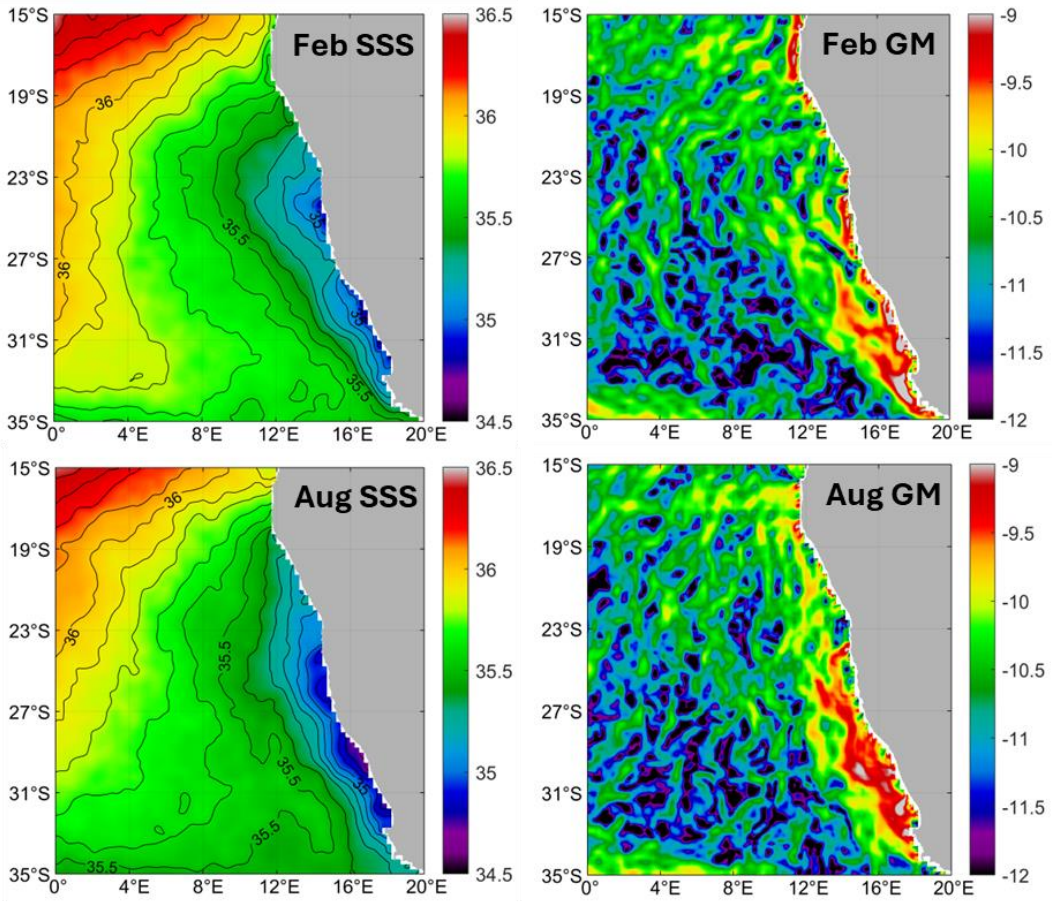

Figure 12. Long-term (2011-2019) mean monthly maps of SSS and log-transformed gradient magnitude (GM) of SSS in mid-summer (February) and mid-winter (August) in the Benguela Upwelling region.

4. Discussion

Large-scale open-ocean fronts: The SMOS SSS data revealed a rich pattern of salinity fronts in the South Atlantic, including a few newly identified features. Perhaps, the most important frontal zone that has been reliably documented during this study is the Tropical Front, which has not been distinguished in the South Atlantic in previous satellite studies of salinity fronts (listed in Section 1 and Table 1). Another newly identified feature of interest is the discontinuity of the Subtropical Frontal Zone (STFZ), which was found to consist of two major frontal zones (Western and Eastern STF), both quasi-zonal yet offset from one another by up to 5° of latitude (roughly 500 km). This finding will likely revive the discussion of continuity (or a possible discontinuity) of the STFZ across the South Atlantic. In this respect, Burls and Reason (2006, p. 10) wrote: "West of about 15°W, the satellite data analysed here suggests little evidence of continuous frontal features associated with the Subtropical Front extending across the basin. By contrast, Deacon [1982] and Peterson and Stramma [1991] used hydrographic data to infer that such a continuous feature does exist across the basin."

Freshwater plumes: Reul et al. (2014) emphasized the importance of SMOS data for monitoring of freshwater plumes of major rivers such as Amazon, Orinoco, and Congo. Reul et al. (2014) also pointed out the importance of monitoring the space-time variability of the freshwater pool created by copious amounts of precipitation in the Inter-Tropical Convergence Zone, ITCZ. River plumes are often bordered by sharp fronts (REFS) that manifest in salinity, temperature, ocean color, water transparency, and turbidity (REFS). The ITCZ freshwater pool is likely bordered by salinity fronts in a pattern similar to that in the equatorial Indian Ocean, where, according to Nyadjro and Subrahmanyam (2016, p. 146), "Strong salinity fronts are observed along the equatorial region, with meridional migration of the fronts following the migration of the Intertropical Convergence Zone

 doi:10.20944/preprints202403.0975.v1

(ITCZ)." However, in the equatorial Atlantic, no salinity fronts associated with the ITCZ have been documented yet.

The **Angola-Benguela Front (ABF)** in the Eastern Tropical Atlantic is traditionally recognized as a boundary between the southward flowing warm waters of the Angola Current and northward flowing cold waters of the Benguela Current (Shannon et al., 1987). The above traditional concept of the ABF as a confluence of two meridional currents is a simplification. Complications come from both sides. In the north, the Congo River's summertime peak discharge feeds the Congo River plume extending south alongshore toward the ABF. In the south, the Benguela upwelling brings cold and less saline water to the surface layer, where this water spreads north alongshore toward the ABF. Thus, the large-scale salinity pattern consists of three water masses: (1) low-salinity water of the Congo River in the north; (2) low-salinity water of the Benguela upwelling in the south; and (3) tropical high-salinity water in-between. The monthly maps of SSS in the Congo-Angola-Benguela region (Figures 9–12) clearly document the significant seasonal and interannual variability of the above three-component SSS pattern. The summertime (January-April) southward alongshore spreading of the Congo River water is apparent in every summer except 2013 and 2017, with the most extensive spreading event in 2016. Perhaps not coincidentally, this was the year of a Benguela Niño. The Benguela upwelling's intensity and extent are known to peak in winter (July-September) when the southerly winds pick up. The northward alongshore spreading of upwelled water normally follows upwelling episodes. The monthly maps of SSS in the Benguela Upwelling region (Figure 12) portray the seasonal northward spreading of low-salinity water brought by upwelling and alongshore advection.

5. Conclusions

We conducted a systematic study of sea surface salinity (SSS) fronts in the South Atlantic using satellite SMOS SSS data from 2011-2019. We used high-resolution (1/20°) daily SSS data generated at the Barcelona Expert Center of Remote Sensing (BEC). The daily data were monthly averaged (largely to mitigate some artifacts, e.g., faint horizontal stripes); then monthly data were used in the analysis. The Belkin-O'Reilly algorithm (BOA) was used to generate gradients of SSS. Zones of high gradient magnitude (GM) of SSS were identified with salinity fronts. To facilitate feature recognition in satellite imagery, the original SSS data has been log-transformed; then, after BOA, the gradient was log-transformed. This technique enhanced visual contrast of gradient maps and brought out a few newly identified features such as a giant 2000-km-long ripple field of quasi-meridional mesoscale (100 km wave length) striations in the tropical-subtropical Atlantic and a narrow linear band of SSS maximum south of the Tropical Front. Large-scale open-ocean salinity fronts are stable and do not substantially change seasonally and interannually, except for the equatorial belt and, to some extent, the Tropical Front, which shifts seasonally in the north-south direction and also changes its orientation (non-zonal tilt). Strongest fronts border low-salinity regions maintained by the Rio de la Plata discharge, Magellan Strait outflow, Congo River discharge, and Benguela upwelling. In the SW Atlantic, the Plata plume expands northward in winter (June-July), reaching into the South Brazilian Bight, up to Cabo Frio (23°S) and beyond. The inner Plata front moves in and out seasonally. The Magellan Strait outflow expands northward in winter (June-July) from 53°S up to 39-40°S and sometimes beyond, approaching the Plata outflow. In the SE Atlantic, the Congo River plume spreads radially from the river mouth, with the outflow direction and areal extent varying seasonally and interannually. The plume is often bordered from the south by a quasi-zonal front along 6°S. The diluted Congo River water spreads southward seasonally down to the Angola-Benguela Front at 16°S (mean position). The Benguela upwelling is bordered by a quasi-meridional front, which extends north alongshore up to 20°S, where the low-salinity Benguela upwelling water forms a salinity front, which is separate from the thermal Angola-Benguela Front at 16°S. The high-salinity tropical water ("Angola water") forms a wedge between the diluted Congo River water and low-salinity Benguela upwelling water. This high-salinity wedge is bordered by salinity fronts that migrate north-south seasonally.

Acknowledgments: We are truly and greatly appreciative of the superb work done at the Barcelona Expert Center of Remote Sensing (BEC), which made this study possible.

References

Acha EM, Mianzan HW, Guerrero RA, Favero M, Bava J, 2004. Marine fronts at the continental shelves of austral South America: Physical and ecological processes. *Journal of Marine Systems*, **44**(1-2), 83-105. https://doi.org/10.1016/j.jmarsys.2003.09.005.

Acha EM, Mianzan H, Guerrero R, Carreto J, Giberto D, Montoya N, Carignan M, 2008. An overview of physical and ecological processes in the Rio de la Plata Estuary. *Continental Shelf Research*, **28**(13), 1579-1588. https://doi.org/10.1016/j.csr.2007.01.031.

Allega L, Pisoni JP, Cozzolino E, Maenza RA, Piccolo MC, 2021. The variability of sea surface temperature in the Patagonian Shelf Argentina, from 35 years of satellite information. *International Journal of Remote Sensing*, **42**(16), 6090-6106. https://doi.org/10.1080/01431161.2021.1934600.

Alsdorf D, Beighley E, Laraque A, Lee H, Tshimanga R, O'Loughlin F, Mahé G, Dinga B, Moukandi G, Spencer RG, 2016. Opportunities for hydrologic research in the Congo Basin. *Reviews of Geophysics*, **54**(2), 378-409. https://doi.org/10.1002/2016RG000517.

Andrews WRH, Hutchings L, 1980. Upwelling in the southern Benguela Current. *Progress in Oceanography*, **9**(1), 1-81. https://doi.org/10.1016/0079-6611(80)90015-4.

Armstrong DA, Mitchell-Innes BA, Verheye-Dua F, Waldron H, Hutchings L, 1987. Physical and biological features across an upwelling front in the southern Benguela. *South African Journal of Marine Science*, **5**(1), 171-190. https://doi.org/10.2989/025776187784522559.

Artana C, Lellouche JM, Park YH, Garric G, Koenig Z, Sennéchael N, Ferrari R, Piola AR, Saraceno M, Provost C, 2018. Fronts of the Malvinas Current System: surface and subsurface expressions revealed by satellite altimetry, Argo floats, and Mercator operational model outputs. *Journal of Geophysical Research: Oceans*, **123**(8), 5261-5285. https://doi.org/10.1029/2018JC013887.

Artana C, Provost C, Lellouche JM, Rio MH, Ferrari R, Sennéchael N, 2019. The Malvinas Current at the Confluence with the Brazil Current: Inferences from 25 years of Mercator Ocean reanalysis. *Journal of Geophysical Research: Oceans*, **124** (10), 7178-7200. https://doi.org/10.1029/2019JC015289.

Asto C, Chaigneau A, Gutiérrez D, 2019. Spatio-temporal variability of the equatorial front in the eastern tropical Pacific from remote sensing salinity data (2010-2015). *Deep-Sea Research Part II*, **169-170**, Article 104640. https://doi.org/10.1016/j.dsr2.2019.104640.

Aubriot L, Zabaleta B, Bordet F, Sienra D, Risso J, Achkar M, Somma A, 2020. Assessing the origin of a massive cyanobacterial bloom in the Río de la Plata (2019): Towards an early warning system. *Water Research*, **181**, Article 115944. https://doi.org/10.1016/j.watres.2020.115944.

Bao SL, Wang HZ, Zhang R, Yan HQ, Chen J, Bai CZ, 2021. Application of phenomena-resolving assessment methods to satellite sea surface salinity products. *Earth and Space Science* **8**(8), Article e2020EA001410. https://doi.org/10.1029/2020EA001410.

Barré N, Provost C, Saraceno M, 2006. Spatial and temporal scales of the Brazil–Malvinas Current confluence documented by simultaneous MODIS Aqua 1.1-km resolution SST and color images. *Advances in Space Research*, **37**(4), 770-786. https://doi.org/10.1016/j.asr.2005.09.026.

Belkin IM, 1993. Frontal structure of the South Atlantic. In: *Pelagic Ecosystems of the Southern Ocean*, edited by N. M. Voronina, pp. 40-53 (in Russian), Nauka, Moscow.

Belkin IM, Gordon AL, 1996. Southern Ocean fronts from the Greenwich meridian to Tasmania. *Journal of Geophysical Research: Oceans*, **101**(C2), 3675-3696. https://doi.org/10.1029/95JC02750.

Belkin IM, O'Reilly JE, 2009. An algorithm for oceanic front detection in chlorophyll and SST satellite imagery. *Journal of Marine Systems*, **78**(3), 317-326. https://doi.org/10.1016/j.jmarsys.2008.11.018.

Belkin, I.M., Cornillon, P.C., Sherman, K., 2009. Fronts in Large Marine Ecosystems. *Progress in Oceanography* **81** (1-4), 223-236. https://doi.org/10.1016/j.pocean.2009.04.015.

Belkin IM, 2021. Remote sensing of ocean fronts in marine ecology and fisheries. *Remote Sensing*, **13**(5), Article 883. https://doi.org/10.3390/rs13050883.

Billany W, Swart S, Hermes J, Reason CJC, 2010. Variability of the Southern Ocean fronts at the Greenwich Meridian. *Journal of Marine Systems*, **82**(4), 304-310. https://doi.org/10.1016/j.jmarsys.2010.06.005.

Borús J, Giacosa J, 2014. Evaluación de Caudales Diarios Descargados Por Los Grandes Ríos Del Sistema Del Plata al Río de La Plata. In: *Direccion y Alerta Hidrológico*, Instituto Nacional del Agua, Ezeiza, Argentina.

Bouali M, Sato OT, Polito PS, 2017. Temporal trends in sea surface temperature gradients in the South Atlantic Ocean. *Remote Sensing of Environment*, **194**, 100-114. https://doi.org/10.1016/j.rse.2017.03.008.

Boutin J, Vergely JL, Marchand S, d'Amico F, Hasson A, Kolodziejczyk N, Reul N, Reverdin G, Vialard J, 2018. New SMOS Sea Surface Salinity with reduced systematic errors and improved variability. *Remote Sensing of Environment*, **214**, 115-134. https://doi.org/10.1016/j.rse.2018.05.022.

Boutin J, Reul N, Köhler J, Martin A, Catany R, Guimbard S, Rouffi F, Vergely JL, Arias M, Chakroun M, Corato G, 2021. Satellite-based sea surface salinity designed for ocean and climate studies. *Journal of Geophysical Research: Oceans*, **126**(11), Article e2021JC017676. https://doi.org/10.1029/2021JC017676.

Boutin J, Yueh S, Bindlish R, Chan S, Entekhabi D, Kerr Y, Kolodziejczyk N, Lee T, Reul N, Zribi M, 2023. Soil moisture and sea surface salinity derived from satellite-borne sensors. *Surveys in Geophysics*, **44**(5), 1449-1487. https://doi.org/10.1007/s10712-023-09798-5.

Brun AA, Ramirez N, Pizarro O, Piola AR, 2020. The role of the Magellan Strait on the southwest South Atlantic shelf. *Estuarine, Coastal and Shelf Science*, **237**, Article 106661. https://doi.org/10.1016/j.ecss.2020.106661.

Burls NJ, Reason CJC, 2006. Sea surface temperature fronts in the midlatitude South Atlantic revealed by using microwave satellite data. *Journal of Geophysical Research: Oceans*, **111**(C8), Article C08001. https://doi.org/10.1029/2005JC003133.

Burrage D, Wesson J, Martinez C, Pérez T, Möller Jr O, Piola A, 2008. Patos Lagoon outflow within the Río de la Plata plume using an airborne salinity mapper: Observing an embedded plume. *Continental Shelf Research*, **28**(13), 1625-1638. https://doi.org/10.1016/j.csr.2007.02.014.

Campbell JW, 1995. The lognormal distribution as a model for bio-optical variability in the sea. *Journal of Geophysical Research*, **100**(C7), 13,237-13,254. https://doi.org/10.1029/95jc00458.

Campos EJD, Lorenzzetti JA, Stevenson MR, Stech JL, de Souza RB, 1996. Penetration of waters from the Brazil–Malvinas Confluence region along the South American continental shelf up to 23°S. *Anais da Academia Brasileira de Ciências*, **68** (Suppl. 1), 49-58.

Campos EJD, Lentini CAD, Miller JL, Piola AR, 1999. Interannual variability of the sea surface temperature in the South Brazil Bight. *Geophysical Research Letters*, **26**(14), 2061-2064. https://doi.org/10.1029/1999GL900297.

Campos EJD, Piola AR, Matano RP, Miller JL, 2008. PLATA: A synoptic characterization of the southwest Atlantic shelf under influence of the Plata River and Patos Lagoon outflows. *Continental Shelf Research*, **28**(13), 1551-1555. https://doi.org/10.1016/j.csr.2008.03.007.

Castellanos P, Olmedo E, Pelegrí JL, Turiel A, Campos EJD, 2019. Seasonal variability of retroflection structures and transports in the Atlantic Ocean as inferred from satellite-derived salinity maps. *Remote Sensing*, **11**(7), Article 802. https://doi.org/10.3390/rs11070802.

Chao Y, Farrara JD, Schumann G, Andreadis KM, Moller D, 2015. Sea surface salinity variability in response to the Congo River discharge. *Continental Shelf Research*, **99**, 35-45. https://doi.org/10.1016/j.csr.2015.03.005.

Chen HH, Qi Y, Wang Y, Chai F, 2019. Seasonal variability of SST fronts and winds on the southeastern continental shelf of Brazil. *Ocean Dynamics*, **69**(11-12), 1387-1399. https://doi.org/10.1007/s10236-019-01310-1.

Combes V, Matano RP, 2018. The Patagonian shelf circulation: Drivers and variability. *Progress in oceanography*, **167**, 24-43. https://doi.org/10.1016/j.pocean.2018.07.003.

Currant-Everett D, 2018. Explorations in statistics: the log transformation. *Advances in Physiology Education*, **42**(2), 343-347. https://doi.org/10.1152/ADVAN.00018.2018.

da Silveira IC, Pereira F, Flierl GR, Simoes-Sousa IT, Palóczy A, Borges-Silva M, Rocha CB, 2023. The Brazil Current quasi-stationary unstable meanders at 22°S–23°S. *Progress in Oceanography*, **210**, Article 102925. https://doi.org/10.1016/j.pocean.2022.102925.

Dávila PM, Figueroa D, Müller M, 2002. Freshwater input into the coastal ocean and its relation with the salinity distribution off austral Chile (35-55°S). *Continental Shelf Research*, **22**(3), 521-534. https://doi.org/10.1016/S0278-4343(01)00072-3.

Denamiel C, Budgell WP, Toumi R, 2013. The Congo River plume: Impact of the forcing on the far-field and near-field dynamics. *Journal of Geophysical Research: Oceans*, **118**(2), 964-989. https://doi.org/10.1002/jgrc.20062.

Dencausse G, Arhan M, Speich S, 2011. Is there a continuous Subtropical Front south of Africa? *Journal of Geophysical Research: Oceans*, **116**(C2), Article C02027. https://doi.org/10.1029/2010JC006587.

Dogliotti AI, Ruddick K, Guerrero R, 2016. Seasonal and inter-annual turbidity variability in the Río de la Plata from 15 years of MODIS: El Niño dilution effect. *Estuarine, Coastal and Shelf Science*, **182**, 27-39. https://doi.org/10.1016/j.ecss.2016.09.013.

Dong S, Sprintall J, Gille ST, 2006. Location of the Antarctic polar front from AMSR-E satellite sea surface temperature measurements. *Journal of Physical Oceanography*, **36**(11), 2075-2089. https://doi.org/10.1175/JPO2973.1.

Donlon CJ, Martin M, Stark J, Roberts-Jones J, Fiedler E, Wimmer W, 2012. The operational sea surface temperature and sea ice analysis (OSTIA) system. *Remote Sensing of Environment*, **116**, 140-158. https://doi.org/10.1016/j.rse.2010.10.017.

Duncombe Rae CM, 2005. A demonstration of the hydrographic partition of the Benguela upwelling ecosystem at 26°40'S. African Journal of Marine Science, 27(3), 617-628. https://doi.org/10.2989/18142320509504122.

Ekau W, Verheye HM, 2005. Influence of oceanographic fronts and low oxygen on the distribution of ichthyoplankton in the Benguela and southern Angola currents. *African Journal of Marine Science*, **27**(3), 629-639. https://doi.org/10.2989/18142320509504123.

Framiñan MB, Brown OB, 1996. Study of the Río de la Plata turbidity front, Part 1: spatial and temporal distribution. *Continental Shelf Research*, **16**(10), 1259-1282. https://doi.org/10.1016/0278-4343(95)00071-2.

Framiñan MB, Etala MP, Acha EM, Guerrero RA, Lasta CA, Brown OB, 1999. Physical characteristics and processes of the Río de la Plata Estuary, in *Estuaries of South America, Their Geomorphology and Dynamics*, edited by Gerardo M. E. Perillo, M. Cintia Piccolo, and Mario Pino-Quivira, pp. 161-194, Springer, Berlin.

Franco BC, Piola AR, Rivas AL, Baldoni A, Pisoni JP, 2008. Multiple thermal fronts near the Patagonian shelf break. *Geophysical Research Letters*, **35**(2), Article L02607. https://doi.org/10.1029/2007GL032066.

Franco BC, Ruiz-Etcheverry LA, Marrari M, Piola AR, Matano RP, 2022. Climate change Impacts on the Patagonian shelf break front. *Geophysical Research Letters*, **49**(4), Article e2021GL096513. https://doi.org/10.1029/2021GL096513.

Freeman NM, Lovenduski NS, 2016. Mapping the Antarctic Polar Front: weekly realizations from 2002 to 2014. *Earth System Science Data*, **8**(1), 191-198. https://doi.org/10.5194/essd-8-191-2016.

Funke M, 2009. On the subtropical front in the South Atlantic Ocean. M.Sc. Thesis. University of Cape Town, 82 pp. http://hdl.handle.net/11427/6473.

Gallagher NC, Wise GL, 1981. A theoretical analysis of the properties of median filters. *IEEE Transactions on Acoustics, Speech, and Signal Processing*, **29**(6), 1136-1141. https://doi.org/10.1109/TASSP.1981.1163708.

Gammelsrød T, Bartholomae CH, Boyer DC, Filipe VLL, O'Toole MJ, 1998. Intrusion of warm surface water along the Angolan-Namibian coast in February–March 1995: the 1995 Benguela Nino. *South African Journal of Marine Science*, **19**(1), 41-56. https://doi.org/10.2989/025776198784126719.

García NO, Vargas WM, 1998. The temporal climatic variability in the 'Río de la Plata' basin displayed by the river discharges. *Climatic Change*, **38**(3), 359-379. https://doi.org/10.1023/A:1005386530866.

Giglio D, Johnson GC, 2016. Subantarctic and Polar Fronts of the Antarctic Circumpolar Current and Southern Ocean heat and freshwater content variability: A view from Argo. *Journal of Physical Oceanography*, **46**(3), 749-768. https://doi.org/10.1175/JPO-D-15-0131.1.

Glorioso PD, 1987. Temperature distribution related to shelf-sea fronts on the Patagonian shelf. *Continental Shelf Research*, **7**(1), 27-34. https://doi.org/10.1016/0278-4343(87)90061-6.

Gonzalez RC, Woods RE, 2018. *Digital Image Processing*, 4th edition. Pearson, London, UK.

Gonzalez RC, Woods RE, Eddins SL, 2020. *Digital Image Processing Using MATLAB®*, 3rd edition. Gatesmark Publishing.

Good S, Fiedler E, Mao CY, Martin MJ, Maycock A, Reid R, Roberts-Jones J, Searle T, Waters J, While J, Worsfold M, 2020. The current configuration of the OSTIA system for operational production of foundation sea surface temperature and ice concentration analyses. *Remote Sensing*, **12**(4), Article 720. https://doi.org/10.3390/rs12040720.

Graham RM, de Boer AM, 2013. The Dynamical Subtropical Front. *Journal of Geophysical Research: Oceans*, **118**(10), 5676-5685. https://doi.org/10.1002/jgrc.20408.

Graham RM, de Boer AM, Heywood KJ, Chapman MR, Stevens DP, 2012. Southern Ocean fronts: Controlled by wind or topography? *Journal of Geophysical Research: Oceans*, **117**(C8), Article C08018. https://doi.org/10.1029/2012JC007887.

Gregg WW, Casey NW, 2004. Global and regional evaluation of the SeaWiFS chlorophyll data set. *Remote Sensing of Environment*, **93**(4), 463-479. https://doi.org/10.1016/j.rse.2003.12.012.

Guerrero RA, Acha EM, Framiñan MB, Lasta CA, 1997. Physical oceanography of the Río de la Plata estuary, Argentina. *Continental Shelf Research*, **17**(7), 727-742. https://doi.org/10.1016/S0278-4343(96)00061-1.

Guerrero RA, Piola AR, Fenco H, Matano RP, Combes V, Chao Y, James C, Palma ED, Saraceno M, Strub PT, 2014. The salinity signature of the cross-shelf exchanges in the Southwestern Atlantic Ocean: Satellite observations. *Journal of Geophysical Research: Oceans*, **119**(11), 7794-7810. https://doi.org/10.1002/2014JC010113.

Guihou K, Piola AR, Palma ED, Chidichimo MP, 2020. Dynamical connections between large marine ecosystems of austral South America based on numerical simulations. *Ocean Science*, **16**(2), 271-290, https://doi.org/10.5194/os-16-271-2020.

Hopkins J, Lucas M, Dufau C, Sutton M, Stum J, Lauret O, Channelliere C, 2013. Detection and variability of the Congo River plume from satellite derived sea surface temperature, salinity, ocean colour and sea level. *Remote Sensing of Environment*, **139**, 365-385. http://dx.doi.org/10.1016/j.rse.2013.08.015.

Hösen E, Möller J, Jochumsen K, Quadfasel D, 2016. Scales and properties of cold filaments in the Benguela upwelling system off Lüderitz. *Journal of Geophysical Research: Oceans*, **121**(3), 1896-1913. https://doi.org/10.1002/2015JC011411.

Houndegnonto OJ, Kolodziejczyk N, Maes C, Bourlès B, Da-Allada CY, Reul N, 2021. Seasonal variability of freshwater plumes in the eastern Gulf of Guinea as inferred from satellite measurements. *Journal of Geophysical Research: Oceans*, **126**, Article e2020JC017041. https://doi.org/10.1029/2020JC017041.

Hutchings L, Armstrong BA, Mitchell-Innes DA, 1986. The frontal zone in the southern Benguela Current. In *Marine Interfaces Eco-Hydrodynamics, Proceedings of the 17th International Liege Colloquium on Ocean Hydrodynamics, Liege, Belgium, 13–17 May 1985*; Nihoul, J.C.J., Ed.; Elsevier Oceanography Series, Volume **42**; Elsevier: Amsterdam, The Netherlands, pp. 67-94. https://doi.org/10.1016/S0422-9894(08)71039-0.

Hutchings L, Van der Lingen CD, Shannon LJ, Crawford RJM, Verheye HMS, Bartholomae CH, Van der Plas AK, Louw D, Kreiner A, Ostrowski M, Fidel Q, 2009. The Benguela Current: An ecosystem of four components. *Progress in Oceanography*, **83**(1-4), 15-32. https://doi.org/10.1016/j.pocean.2009.07.046.

Imbol Koungue RA, Brandt P, Lübbecke J, Prigent A, Martins MS, Rodrigues RR, 2021. The 2019 Benguela Niño. *Frontiers in Marine Science*, **8**, Article 800103. https://doi.org/10.3389/fmars.2021.800103.

Irons JR, Petersen GW, 1981. Texture transforms of remote sensing data. *Remote Sensing of Environment*, **11**(C), 359-370. https://doi.org/10.1016/0034-4257(81)90033-X.

Jarugula S, McPhaden MJ, 2023. Indian Ocean Dipole affects eastern tropical Atlantic salinity through Congo River Basin hydrology. *Communications Earth & Environment*, **4**(1), Article 366. https://doi.org/10.1038/s43247-023-01027-6.

Juliano MF, Alves ML, 2007. The Atlantic subtropical front/current systems of Azores and St. Helena. *Journal of Physical Oceanography*, **37**(11), 2573-2598. https://doi.org/10.1175/2007JPO3150.1.

Kao HY, Lagerloef GSE, 2015. Salinity fronts in the tropical Pacific Ocean, *Journal of Geophysical Research: Oceans*, **120**(2), 1096-1106. https://doi.org/10.1002/2014JC010114.

Kerr YH, Waldteufel P, Wigneron JP, Delwart S, Cabot F, Boutin J, Escorihuela MJ, Font J, Reul N, Gruhier C, Juglea SE, Drinkwater MR, Hahne A, Martín-Neira M, Mecklenburg S, 2010. The SMOS mission: New tool for monitoring key elements of the global water cycle. *Proceedings of the IEEE*, **98**(5), 666-687. https://doi.org/10.1109/JPROC.2010.2043032.

Kim YS, Orsi AH, 2014. On the variability of Antarctic Circumpolar Current fronts inferred from 1992–2011 altimetry. *Journal of Physical Oceanography*, **44**(12), 3054-3071. https://doi.org/10.1175/JPO-D-13-0217.1.

Kolodziejczyk N, Hernandez O, Boutin J, Reverdin G, 2015. SMOS salinity in the subtropical North Atlantic salinity maximum: 2. Two-dimensional horizontal thermohaline variability. *Journal of Geophysical Research: Oceans*, **120**(2), 972-987. https://doi.org/10.1002/2014JC010103.

Kruk C, Martínez A, de la Escalera GM, Trinchin R, Manta G, Segura AM, Piccini C, Brena B, Yannicelli B, Fabiano G, Calliari D, 2021. Rapid freshwater discharge on the coastal ocean as a mean of long distance spreading of an unprecedented toxic cyanobacteria bloom. *Science of The Total Environment*, **754**, Article 142362. https://doi.org/10.1016/j.scitotenv.2020.142362.

Laraque A, Moukandi N'kaya GD, Orange D, Tshimanga R, Tshitenge JM, Mahé G, Nguimalet CR, Trigg MA, Yepez S, Gulemvuga G, 2020. Recent budget of hydroclimatology and hydrosedimentology of the Congo River in Central Africa. *Water*, **12**(9), Article 2613. https://doi.org/10.3390/w12092613.

Lass HU, Schmidt M, Mohrholz V, Nausch G, 2000. Hydrographic and current measurements in the area of the Angola–Benguela front. *Journal of Physical Oceanography*, **30**(10), 2589-2609. https://doi.org/10.1175/1520-0485(2000)030<2589:HACMIT>2.0.CO;2.

Legeckis R, 1978. A survey of worldwide sea surface temperature fronts detected by environmental satellites. *Journal of Geophysical Research: Oceans*, **83**(C9), 4501-4522. https://doi.org/10.1029/JC083iC09p04501.

Legeckis R, Gordon AL, 1982. Satellite observations of the Brazil and Falkland currents— 1975 1976 and 1978. *Deep-Sea Research*, **29**(3), 375-401. https://doi.org/10.1016/0198-0149(82)90101-7.

Lisboa PV, Fernandes EH, Sottolichio A, Huybrechts N, Bendo AR, 2022. Coastal plumes contribution to the suspended sediment transport in the Southwest Atlantic inner continental shelf. *Journal of Marine Systems*, **236**, Article 103796.

Lorenzzetti JA, Stech JL, Mello Filho WL, Assireu AT, 2009. Satellite observation of Brazil Current inshore thermal front in the SW South Atlantic: Space/time variability and sea surface temperatures. *Continental Shelf Research*, **29**(17), 2061-2068. https://doi.org/10.1016/j.csr.2009.07.011.

Luko CD, da Silveira ICA, Simoes-Sousa IT, Araujo JM, Tandon A, 2021. Revisiting the Atlantic South Equatorial Current. *Journal of Geophysical Research: Oceans*, **126**(7), Article e2021JC017387. https://doi.org/10.1029/2021JC017387.

Lutjeharms JRE, Meeuwis JM, 1987. The extent and variability of South-East Atlantic upwelling. *South African Journal of Marine Science*, **5**(1), 51-62. https://doi.org/10.2989/025776187784522621.

Lutjeharms JRE, Valentine HR, 1984. Southern Ocean thermal fronts south of Africa. *Deep-Sea Research*, **31**(12), 1461-1475. https://doi.org/10.1016/0198-0149(84)90082-7.

Lutjeharms JRE, Valentine HR, van Ballegooyen RC, 1993. On the Subtropical Convergence in the South Atlantic Ocean. *South African Journal of Science*, **89**(11-12), 552-559.

Maciel FP, Santoro PE, Pedocchi F, 2021. Spatio-temporal dynamics of the Río de la Plata turbidity front; combining remote sensing with in-situ measurements and numerical modeling. *Continental Shelf Research*, **213**, Article 104301. https://doi.org/10.1016/j.csr.2020.104301.

Marta-Almeida M, Dalbosco A, Franco D, Ruiz-Villarreal M, 2021. Dynamics of river plumes in the South Brazilian Bight and South Brazil. *Ocean Dynamics*, **71**(1), 59-80. https://doi.org/10.1007/s10236-020-01397-x.

Martins MS, Stammer D, 2022. Interannual variability of the Congo River Plume-induced sea surface salinity. *Remote Sensing*, **14**(4), Article 1013. https://doi.org/10.3390/rs14041013.

Meeuwis JM, 1991. Geographic characteristics of circulation patterns and features in the South Atlantic and South Indian Oceans using satellite remote sensing. PhD Thesis, University of Johannesburg, 418 pp. https://hdl.handle.net/10210/10106. Accessed 2024-01-14.

Meeuwis JM, Lutjeharms JRE, 1990. Surface thermal characteristics of the Angola-Benguela front. *South African Journal of Marine Science*, **9**(1), 261-279. https://doi.org/10.2989/025776190784378772.

Melnichenko O, Hacker P, Maximenko N, Lagerloef G, Potemra J, 2016. Optimum interpolation analysis of Aquarius sea surface salinity. *Journal of Geophysical Research: Oceans*, **121**(1), 602-616. https://doi.org/10.1002/2015JC011343.

Minnett PJ, Alvera-Azcárate A, Chin TM, Corlett GK, Gentemann CL, Karagali I, Li X, Marsouin A, Marullo S, Maturi E, Santoleri R, Saux Picart S, Steele M, Vazquez-Cuervo J, 2019. Half a century of satellite remote sensing of sea-surface temperature. *Remote Sensing of Environment*, **233**, Article 111366. https://doi.org/10.1016/j.rse.2019.111366.

Mohrholz V, Schmidt M, Lutjeharms JRE, John HC, 2004. Space–time behaviour of the Angola–Benguela Frontal Zone during the Benguela Niño of April 1999. *International Journal of Remote Sensing*, **25**(7-8), 1337-1340. https://doi.org/10.1080/01431160310001592265.

Möller Jr. OO, Piola AR, Freitas AC, Campos EJD, 2008. The effects of river discharge and seasonal winds on the shelf off southeastern South America. *Continental Shelf Research*, **28**(13), 1607-1624. https://doi.org/10.1016/j.csr.2008.03.012.

Moore JK, Abbott MR, Richman JG, 1997. Variability in the location of the Antarctic Polar Front (90°–20°W) from satellite sea surface temperature data. *Journal of Geophysical Research: Oceans*, **102**(C13), 27,825-27,833. https://doi.org/10.1029/97JC01705.

Moore JK, Abbott MR, Richman JG, 1999. Location and dynamics of the Antarctic Polar Front from satellite sea surface temperature data. *Journal of Geophysical Research: Oceans*, **104**(C2), 3059-3073. https://doi.org/10.1029/1998JC900032.

Moreira D, Simionato C, 2019. The Río de la Plata estuary hydrology and circulation. *Meteorologica*, **44**(1), 1-30.

Muelbert JH, Acha M, Mianzan H, Guerrero R, Reta R, Braga ES, Garcia VMT, Berasategui A, Gomez-Erache M, Ramírez F, 2008. Biological, physical and chemical properties at the Subtropical Shelf Front Zone in the SW Atlantic Continental Shelf. *Continental Shelf Research*, **28**(13), 1662-1673. https://doi.org/10.1016/j.csr.2007.08.011.

Muller AA, Mohrholz V, Schmidt M, 2013. The circulation dynamics associated with a northern Benguela upwelling filament during October 2010. *Continental Shelf Research*, **63**, 59-68. https://doi.org/10.1016/j.csr.2013.04.037.

Munzimi YA, Hansen MC, Asante KO, 2019. Estimating daily streamflow in the Congo Basin using satellite-derived data and a semi-distributed hydrological model. *Hydrological Sciences Journal*, **64**(12), 1472-1487. https://doi.org/10.1080/02626667.2019.1647342.

Nyadjro ES, Subrahmanyam B, 2016. Spatial and temporal variability of central Indian Ocean salinity fronts observed by SMOS. *Remote Sensing of Environment*, **180**, 146-153. https://doi.org/10.1016/j.rse.2016.02.049.

Olmedo E, González-Haro C, Hoareau N, Umbert M, González-Gambau V, Martínez J, Gabarró C, Turiel A, 2021. Nine years of SMOS sea surface salinity global maps at the Barcelona Expert Center. *Earth System Science Data*, **13**(2), 857-888. https://doi.org/10.5194/essd-13-857-2021.

Olson DB, Podestá GP, Evans RH, Brown OB, 1988. Temporal variations in the separation of Brazil and Malvinas Currents. *Deep Sea Research*, **35**(12), 1971-1990. https://doi.org/10.1016/0198-0149(88)90120-3.

Palma ED, Matano RP, Piola AR, 2008. A numerical study of the Southwestern Atlantic Shelf circulation: Stratified ocean response to local and offshore forcing. *Journal of Geophysical Research: Oceans*, **113**(C11), Article C11010, https://doi.org/10.1029/2007JC004720.

Palma ED, Matano RP, 2012. A numerical study of the Magellan Plume. *Journal of Geophysical Research: Oceans*, **117**(C5), Article C05041. https://doi.org/10.1029/2011JC007750.

Palma ED, Matano RP, Tonini MH, Martos P, Combes V, 2020. Dynamical analysis of the oceanic circulation in the Gulf of San Jorge, Argentina. *Journal of Marine Systems*, **203**, Article 103261. https://doi.org/10.1016/j.jmarsys.2019.103261.

Peterson RG, Stramma L, 1991. Upper-level circulation in the South Atlantic Ocean. *Progress in Oceanography*, **26**(1), 1-73. https://doi.org/10.1016/0079-6611(91)90006-8.

Peterson RG, Whitworth III T, 1989. The Subantarctic and Polar Fronts in relation to deep water masses through the southwestern Atlantic. *Journal of Geophysical Research: Oceans*, 94(C8), 10,817-10,838. https://doi.org/10.1029/JC094iC08p10817.

Phillipson L, Toumi R, 2019. Assimilation of satellite salinity for modelling the Congo River plume. *Remote Sensing*, **12**(1), Article 11. https://doi.org/10.3390/rs12010011.

Piola AR, Romero SI, 2004. Space-time variability of the Plata River Plume. *Gayana (Concepción)* **68**(2), 482-486. https://doi.org/10.4067/S0717-65382004000300030.

Piola AR, Campos EJD, Möller Jr. OO, Charo M, Martinez C, 2000. Subtropical shelf front off eastern South America. *Journal of Geophysical Research: Oceans*, **105**(C3), 6566-6578. https://doi.org/10.1029/1999jc000300.

Piola AR, Matano RP, Palma ED, Möller Jr OO, Campos EJD, 2005. The influence of the Plata River discharge on the western South Atlantic shelf. *Geophysical Research Letters*, **32**(1), Article L01603. https://doi.org/10.1029/2004GL021638.

Piola AR, Romero SI, Zajaczkovski U, 2008a. Space-time variability of the Plata plume inferred from ocean color. *Continental Shelf Research*, **28**(13), 1556-1567. https://doi.org/10.1016/j.csr.2007.02.013.

Piola AR, Möller Jr. OO, Guerrero RA, Campos EJD, 2008b. Variability of the subtropical shelf front off eastern South America: Winter 2003 and summer 2004. *Continental Shelf Research*, **28**(13), 1639-1648. https://doi.org/10.1016/j.csr.2008.03.013.

Piola AR, Palma ED, Bianchi AA, Castro BM, Dottori M, Guerrero RA, Marrari M, Matano RP, Möller OO, Saraceno M, 2018. Physical oceanography of the SW Atlantic Shelf: A review. In: *Plankton Ecology of the Southwestern Atlantic: From the Subtropical to the Subantarctic Realm*, edited by Mónica S. Hoffmeyer, Marina E. Sabatini, Frederico P. Brandini, Danilo L. Calliari, and Norma H. Santinelli. Springer Cham, pp. 37-56. https://doi.org/10.1007/978-3-319-77869-3_2.

Provost C, Garçon V, Falcon LM, 1996. Hydrographic conditions in the surface layers over the slope-open ocean transition area near the Brazil-Malvinas confluence during austral summer 1990. *Continental Shelf Research*, **16**(2), 215-235. https://doi.org/10.1016/0278-4343(95)00006-M.

Qu TD, Song YT, Maes C, 2014. Sea surface salinity and barrier layer variability in the equatorial Pacific as seen from Aquarius and Argo. *Journal of Geophysical Research: Oceans*, **119**(1), 15-29. https://doi.org/10.1002/2013JC009375.

Reul N, Fournier S, Boutin J, Hernandez O, Maes C, Chapron B, Alory G, Quilfen Y, Tenerelli J, Morisset S, Kerr Y, 2014. Sea surface salinity observations from space with the SMOS satellite: A new means to monitor the marine branch of the water cycle. *Surveys in Geophysics*, **35**(3), 681-722. https://doi.org/10.1007/s10712-013-9244-0.

Reul N, Grodsky SA, Arias M, Boutin J, Catany R, Chapron B, d'Amico F, Dinnat E, Donlon C, Fore A, Fournier S, 2020. Sea surface salinity estimates from spaceborne L-band radiometers: An overview of the first decade of observation (2010–2019). *Remote Sensing of Environment*, **242**, Article 111769. https://doi.org/10.1016/j.rse.2020.111769.

Rivas AL, 2010. Spatial and temporal variability of satellite-derived sea surface temperature in the southwestern Atlantic Ocean. *Continental Shelf Research*, **30**(7), 752-760. https://doi.org/10.1016/j. csr.2010.01.009.

Rivas AL, Pisoni JP, 2010. Identification, characteristics and seasonal evolution of surface thermal fronts in the Argentinean Continental Shelf. *Journal of Marine Systems*, **79**(1-2), 134-143. https://doi.org/10.1016/j.jmarsys.2009.07.008.

Ruiz-Etcheverry LA, Saraceno M, 2020. Sea level trend and fronts in the South Atlantic Ocean. *Geosciences*, **10**(6), Article 218. https://doi.org/10.3390/geosciences10060218.

Saraceno M, Provost C, Piola AR, Bava J, Gagliardini A, 2004. Brazil Malvinas Frontal System as seen from 9 years of advanced very high resolution radiometer data. *Journal of Geophysical Research: Oceans*, **109**(C5), Article C05027. https://doi.org/10.1029/2003JC002127.

Saraceno M, Provost C, Piola AR, 2005. On the relationship between satellite-retrieved surface temperature fronts and chlorophyll *a* in the western South Atlantic. *Journal of Geophysical Research: Oceans*, **110**(C11), Article C11016. https://doi.org/10.1029/2004JC002736.

Shannon LV, Agenbag JJ, Buys MEL, 1987. Large- and mesoscale features of the Angola-Benguela front. *South African Journal of Marine Science*, **5**(1), 11-34, https://doi.org/10.2989/025776187784522261.

Simionato CG, Nuñez MN, Engel M, 2001. The salinity front of the Río de la Plata - A numerical case study for winter and summer conditions. *Geophysical Research Letters*, **28**(13), 2641-2644. https://doi.org/10.1029/2000GL012478.

Smythe-Wright D, Chapman P, Duncombe Rae C, Shannon LV, Boswell SM, 1998. Characteristics of the South Atlantic subtropical frontal zone between 15°W and 5°E. *Deep-Sea Research Part I*, **45**(1), 167-192. https://doi.org/10.1016/S0967-0637(97)00068-X.

Sorí R, Nieto R, Vicente-Serrano SM, Drumond A, Gimeno L, 2017. A Lagrangian perspective of the hydrological cycle in the Congo River basin. *Earth System Dynamics*, **8**(3), 653-675. https://doi.org/10.5194/esd-8-653-2017.

Stramma L, Peterson RG, 1990. The South Atlantic Current. *Journal of Physical Oceanography*, **20**(6), 846-859. https://doi.org/10.1175/1520-0485(1990)020<0846:TSAC>2.0.CO;2.

Trathan PN, Brandon MA, Murphy EJ, 1997. Characterization of the Antarctic Polar Frontal Zone to the north of South Georgia in summer 1994. *Journal of Geophysical Research: Oceans*, **102**(C5), 10,483-10,497. https://doi.org/10.1029/97JC00381.

Vazquez-Cuervo J, García-Reyes M, Gómez-Valdés J, 2023. Identification of sea surface temperature and sea surface salinity fronts along the California Coast: Application using Saildrone and satellite derived products. *Remote Sensing*, **15**, Article 484. https://doi.org/10.3390/rs15020484.

Veitch JA, Florenchie P, Shillington FA, 2006. Seasonal and interannual fluctuations of the Angola-Benguela Frontal Zone (ABFZ) using 4.5 km resolution satellite imagery from 1982 to 1999. *International Journal of Remote Sensing*, **27**(5), 987-998. https://doi.org/10.1080/01431160500127914.

Vianna ML, Menezes VV, 2011. Double-celled subtropical gyre in the South Atlantic Ocean: Means, trends, and interannual changes. *Journal of Geophysical Research: Oceans*, **116**(C3), Article C03024. https://doi.org/10.1029/2010JC006574.

Vic C, Berger H, Tréguier AM, Couvelard X, 2014. Dynamics of an equatorial river plume: Theory and numerical experiments applied to the Congo plume case. *Journal of Physical Oceanography*, **44**(3), 980-994. https://doi.org/10.1175/JPO-D-13-0132.1.

Vinogradova N, Lee T, Boutin J, Drushka K, Fournier S, Sabia R, Stammer D, Bayler E, Reul N, Gordon A, Melnichenko O, Li LF, Hackert E, Martin M, Kolodziejczyk N, Hasson A, Brown S, Misra S, Lindstrom E,

 doi:10.20944/preprints202403.0975.v1

2019. Satellite salinity observing system: Recent discoveries and the way forward. *Frontiers in Marine Science*, **6**, Article 243. https://doi.org/10.3389/fmars.2019.00243.

Vizy EK, Cook KH, Sun X, 2018. Decadal change of the South Atlantic Ocean Angola-Benguela frontal zone since 1980. *Climate Dynamics*, **51**(9-10), 3251-3273, https://doi.org/10.1007/s00382-018-4077-7.

von Bodungen B, John HC, Lutjeharms JRE, Mohrholz V, Veitch J, 2008. Hydrographic and biological patterns across the Angola–Benguela Frontal Zone under undisturbed conditions. *Journal of Marine Systems*, **74**(1-2), 189-215. https://doi.org/10.1016/j.jmarsys.2007.12.007.

Wang Z, Chen G, Han Y, Ma CY, Lv M, 2021. Southwestern Atlantic Ocean fronts detected from satellite-derived SST and chlorophyll. *Remote Sensing*, **13**(21), Article 4402. https://doi.org/10.3390/rs13214402.

Wang Z, Chen G, Ma CY, Liu YL, 2023. Southwestern Atlantic Ocean fronts detected from the fusion of multi-source remote sensing data by a deep learning model. *Frontiers in Marine Science*, **10**, Article 1140645. https://doi.org/10.3389/fmars.2023.1140645.

Werdell PJ, McKinna LIW, Boss E, Ackleson SG, Craig SE, Gregg WW, Lee ZP, Maritorena S, Roesler CS, Rousseaux CS, Stramski D, Sullivan JM, Twardowski MS, Tzortziou M, Zhang XD, 2018. An overview of approaches and challenges for retrieving marine inherent optical properties from ocean color remote sensing. *Progress in Oceanography*, **160**, 186-212. https://doi.org/10.1016/j.pocean.2018.01.001.

Wongchuig S, Kitambo B, Papa F, Paris A, Fleischmann AS, Gal L, Boucharel J, Paiva R, Oliveira RJ, Tshimanga RM, Calmant S, 2023. Improved modeling of Congo's hydrology for floods and droughts analysis and ENSO teleconnections. *Journal of Hydrology: Regional Studies*, **50**, Article 101563. https://doi.org/10.1016/j.ejrh.2023.101563.

Yu LS, 2015. Sea-surface salinity fronts and associated salinity-minimum zones in the tropical ocean. *Journal of Geophysical Research: Oceans*, **120**(6), 4205-4225. https://doi.org/10.1002/2015JC010790.

Zhang F, Li XF, Hu JY, Sun ZY, Zhu J, Chen ZZ, 2014. Summertime sea surface temperature and salinity fronts in the southern Taiwan Strait. *International Journal of Remote Sensing*, **35**(11-12), 4452-4466. https://doi.org/10.1080/01431161.2014.916454.